The Polarity Protein VANG-1 Antagonizes Wnt Signaling by Facilitating Frizzled Endocytosis

Chun-Wei He[1], Chien-Po Liao[1,*], Chung-Kuan Chen[1,*‡], Jérôme Teulière[2], Chun-Hao Chen[1,#], Chun-Liang Pan[1,§]

[1]Institute of Molecular Medicine, College of Medicine, National Taiwan University, Taipei 10002, Taiwan

[2]Department of Molecular Cell Biology, University of California, Berkeley, CA94720-3204, USA

[*] Equal contribution

[‡] Present address: Program in Biomedical Sciences, Graduate School of Comprehensive Human Sciences, University of Tsukuba, Tsukuba, Ibaraki 305-8575, Japan

[#] Present address: Division of Biology and Bioengineering, California Institute of Technology, Pasadena, CA91125, USA

[§] Correspondence

Corresponding author: Chun-Liang Pan,

Institute of Molecular Medicine, College of Medicine, National Taiwan University,

No.7 Chung-Shan South Road, Taipei 10002, Taiwan

E-mail: chunliangpan@gmail.com

Phone: 886-2-23123456 ext 88360

Fax: 886-2-23221675

Key words: *C. elegans*, Wnt signaling, planar polarity, neuronal migration, endocytosis, Frizzled

Summary Statement

Fine tuning of signaling transduction ensures fidelity in animal development. The authors find that a cell polarity protein tempers signals that promote neuronal migration by recycling the receptors from the neuronal membrane.

ABSTRACT

Signaling that instructs the migration of neurons needs to be tightly regulated to ensure precise positioning of neurons and subsequent wiring of the neuronal circuits. Wnt-Frizzled signaling controls neuronal migration in metazoans, in addition to many other aspects of neural development. We show that *Caenorhabditis elegans* VANG-1/ Vangl2, a membrane protein that acts in the planar cell polarity (PCP) pathway, antagonizes Wnt signaling by facilitating endocytosis of the Frizzled receptors. Mutations of *vang-1* suppress migration defects of multiple classes of neurons in the *Frizzled* mutants, and overexpression of *vang-1* causes neuronal migration defects similar to those of the Frizzled mutants. Our genetic experiments suggest that VANG-1 facilitates Frizzled endocytosis through β-arrestin2. Coimmunoprecipitation experiments indicate that Frizzled proteins and VANG-1 form a complex, and this physical interaction requires the Frizzled cysteine-rich domain (CRD). Our work reveals a novel mechanism mediated by the PCP protein VANG-1 that downregulates Wnt signaling through Frizzled endocytosis.

INTRODUCTION

Wiring of the nervous system during development is established first by neuronal migration, followed by navigation of axon growth cones towards their innervation targets and subsequent axon branching and synapse formation. The migration of neurons and axon growth cones is regulated by highly dynamic signals in the environment that function as attractive or repulsive cues (Tessier-Lavigne and Goodman, 1996). Over the past three decades, several classes of conserved neuronal guidance cues had been uncovered, including Netrin, Slit, semaphorins, ephrins, Sonic Hedgehog and Wnt glycoproteins (Tessier-Lavigne and Goodman, 1996; Blockus and Chedotal, 2016; Dudanova and Klein, 2013; Jongbloets and Pasterkamp, 2014;Sun et al., 2011; Yam and Charron, 2013). While substantial efforts had been dedicated to deciphering the signaling pathways through which these factors instruct neuronal and growth cone migration, little is known about the regulatory mechanisms that downregulate them to prevent prolonged, aberrant signaling that could lead to guidance errors.

The availability of receptors on the plasma membrane is a well-established regulatory mechanism that modulates the magnitude and duration of signaling. In *Drosophila* embryo, trafficking of the Robo receptor to the growth cone membrane of pre-crossing commissural axons is prevented by the Golgi protein Commissureless, which traps Robo in the Golgi (Keleman et al., 2002; Tear et al., 1996; Kidd et al., 1998). In the *Commissureless* mutant, constitutive Robo availability on the axonal membrane inadvertently transmits repulsive signaling by binding the Slit ligand, preventing the commissural axons from crossing the midline and hence causing the “commissureless” axonal phenotype (Keleman et al., 2002;Kidd et al., 1998;Tear et al., 1996). Recent studies suggest that internalization of Frizzleds, seven-pass transmemebrane proteins that function as Wnt receptors, modulates Wnt signaling and regulates axon guidance in *C. elegans* and rodents. Depending on the cellular contexts, Frizzled internalization may activate or terminate Wnt signaling. For

example, internalization of Frizzleds triggered by the PLR-1 E3 ligase-mediated ubiquitination downregulates Wnt signaling to ensure proper axon development in *C. elegans* (Moffat et al., 2014), consistent with the vertebrate PLR-1 homologue ZNRF3/RNF43 downregulating Frizzleds and inhibiting Wnt signaling in the mouse intestinal epithelium (Koo et al., 2012). Frizzled internalization could also activate Wnt signaling. In the mouse spinal cord, Vangl2, a four-pass transmembrane protein of the Planar Cell Polarity (PCP) pathway, facilitates Frizzled endocytosis by antagonizing hyperphosphorylation of Frizzleds mediated by Dvl1/Dishevelled. In this context, Frizzled internalization activates Wnt signaling and promotes proper axon guidance (Shafer et al., 2011). Consistent with this, we recently showed that *C. elegans* VANG-1/Vangl2 promotes Wnt signaling by facilitating Frizzled internalization to instruct neurite branching patterns in the PLM mechanosensory neuron (Chen et al., 2017).

The aforementioned findings reveal an important, cell-autonomous function of Vangl2 in promoting Wnt signaling, in contrast to its complex non-autonomous requirement in *Drosophila* embryonic epithelia that involves interaction with Frizzleds in the neighboring cells (Bailly et al., 2017; Devenport, 2014). To explore how Vangl2 tunes Wnt signaling to regulate neuronal development, and whether Vangl2-dependent Frizzled internalization occurs in broader, more diverse cellular contexts, we systemically analyze the functions of *C. elegans vang-1* gene in multiple classes of migrating *C. elegans* neurons. In contrast to the regulation of Frizzleds in the non-migrating PLM neuron, we find that VANG-1 antagonizes Wnt signaling by facilitating Frizzled endocytosis in all these migrating neuronal classes. These observations expand the phenotypic repertoire through which VANG-1/Vangl2 modulates Wnt signaling to precisely pattern neuronal migration.

RESULTS

VANG-1 antagonizes Wnt signaling in QL descendant migration in *C. elegans*

The *C. elegans* Q neuroblasts are born in early first larval (L1) stage at equivalent positons on the right (hereafter as QR) and the left side (hereafter as QL) of the worm body. The posterior migration of QL descendants (QL.d) during early L1 requires the *Abdominal-A* family Hox gene *mab-5*, whose expression in the QL lineage is controlled by a β-catenin-dependent Wnt signaling pathway (Fig. 1A,B) (Clark et al., 1993; Wang et al., 1993; Harris et al., 1996; Whangbo and Kenyon, 1999; Korswagen, 2002). Critical genes in this pathway that are essential for *mab-5* activation include *egl-20/Wnt*, *mig-1/Frizzled*, *lin-17/Frizzled*, *mig-5/Dishevelled*, *bar-1 β-catenin*, and the TCF transcription factor *pop-1* (Harris et al., 1996; Eisenmann and Kim, 2000; Korswagen et al., 2000). Loss-of-function mutations of these genes diminish *mab-5* expression and result in reversed, anterior migration of the QL.d, including the PVM (QL.paa) (Fig. 1C,D).

Interestingly, we found that the *tm1422* deletion mutation of *vang-1*, the *C. elegans* homologue of the PCP gene *van Gogh/Strabismus/Vangl2*, suppressed PVM migration defects of the *mig-1* mutant, while it did not affect PVM migration in the otherwise wild-type background (Fig. 1C,D). Similar suppression of PVM defects was seen with another *vang-1* deletion allele, *ok1142*, and also with *vang-1* feeding RNAi (Fig. S1A). In contrast to its significant suppression of the *mig-1* phenotypes, the *vang-1(tm1422)* mutation failed to suppress PVM migration defects in the *egl-20/Wnt*, *mig-5/Dishevelled* and *bar-1/β-catenin* mutants (Fig. 1D). *egl-20*, *mig-5* or *bar-1* represents the single homologue for *Wnt*, *Dishevelled* or *β-catenin*, respectively, that is required for the posterior migration of QL.d. We hypothesize that *vang-1* antagonizes Wnt signaling specifically at the level of Frizzled receptors. Therefore, PVM defects caused by the absence of Wnt ligand (*egl-20*) or signals downstream of Frizzleds (*mig-5* and *bar-1*) are refractory to the effects of *vang-1* mutations.

By contrast, LIN-17, another Frizzled, is also required to promote QL.d migration (Harris et al., 1996; Zinovyeva et al., 2008), and we speculate that restoration of PVM migration in the *mig-1; vang-1* double mutant could be mediated by Wnt signaling through the remaining LIN-17 receptor. This hypothesis predicts that the *vang-1* mutation is not able to suppress QL.d defects in the *mig-1 lin-17* double mutant, which lacks all relevant Frizzled receptors for QL.d migration. Consistent with this hypothesis, the *vang-1* mutation improved PVM defects of the *lin-17* single mutant but failed to do so in the *mig-1 lin-17* double *Frizzled* mutant (Figs. 1D and S2).

Expressing *vang-1* in the Q lineages of the *mig-1; vang-1* mutant, using the *egl-17* promoter, completely reversed the suppression of PVM mismigration conferred by the *vang-1* mutation (Fig. 1E). Furthermore, overexpressing *vang-1* in the QL.d resulted in PVM migration defects in the wild type and enhanced the PVM defects of the *mig-1* mutant (Fig. 1E). These results suggest that *vang-1* antagonizes Wnt signaling cell-autonomously in the QL.d neuroblasts. We confirmed this result by using somatic CRISPR-Cas9 (Clustered Regularly Interspaced Short Palindromic Repeats-Cas9) gene editing (Fig. S1B) (Shen et al., 2014). In brief, we expressed Cas9 under the *egl-17* promoter together with ubiquitously expressed *vang-1* sgRNAs. Mutations of *vang-1* in the Q lineages significantly suppressed PVM defects of the *mig-1* mutant, confirming that *vang-1* acts in the Q lineage (Fig. S1B).

On the basis of the hypothesis that *vang-1* antagonizes *mig-1* functions, we predict that the expression of *mab-5*, the transcriptional target of Wnt signaling in QL.d migration, is restored in the *mig-1; vang-1* double mutant. This is indeed the case: *mab-5* expression in the QL.d was significantly increased in *mig-1; vang-1* compared to that in the *mig-1* mutant, which was barely detectable (Fig. 1F,G). By contrast, the *vang-1* mutation failed to restore *mab-5* expression in the *egl-20* mutant (Fig. 1F,G). Of note, the *vang-1* mutant showed significantly higher level of *mab-5* expression compared to the wild type, consistent with *vang-1* being a negative regulator of Wnt signaling (Fig. 1F,G). Taken together, we conclude

that VANG-1 antagonizes Wnt signaling cell-autonomously at the level of Frizzled receptors during QL.d migration.

We hypothesize that the antagonistic function of *vang-1* in Wnt signaling is broadly conserved in early *C. elegans* neuronal development. Below we test this idea in three additional neuronal contexts: QR descendant (QR.d) migration, hermaphrodite-specific neuron (HSN) migration, and ALM touch neuron polarization.

VANG-1 antagonizes Wnt signaling in QR descendant migration in *C. elegans*

In contrast to QL.d, QR.d migrate to the anterior, and these anterior migration events depend on Wnt signaling genes that are largely distinct from those involved in QL.d migration (Harris et al., 1996; Forrester et al., 2004; Zinovyeva et al., 2008). Specifically, in addition to *egl-20/Wnt*, *cwn-1/Wnt*, *mom-5/Frizzled* and *dsh-2/Dishevelled* promote QR.d anterior migration, while *mig-1/Frizzled*, *mig-5/Dishevelled* or *bar-1/β-catenin* are not required (Maloof et al., 1999; Zinovyeva et al., 2008). Additional Wnt receptors, such as LIN-17 and CFZ-2, are hypothesized to function with MOM-5 in QR.d migration, since QR.d migration defects in the *mom-5* mutant are less severe than those of the *cwn-1; egl-20* double mutant (Forrester et al., 2004; Zinovyeva et al., 2008). Consistent with previous studies, we found that AVM, one of the QR.d, terminated their anterior migration prematurely in the *cwn-1/Wnt*, *egl-20/Wnt*, and *mom-5/Frizzled* mutants (Fig. 2A,B). The *vang-1* mutation ameliorated AVM migration defects in the *egl-20*, *cwn-1* and *mom-5* mutants, and caused the AVM to be more anterior in otherwise wild-type background (Fig. 2A,B). Improvement of QR.d migration by the *vang-1* mutation likely result from Wnt signaling mediated by remaining Wnts or Frizzled receptors in respective single mutants, similar to the suppression of QL.d defects in the *mig-1* mutant (see above). By contrast, the *vang-1* mutation failed to suppress AVM defects caused by the mutation of *mig-14*, the *C. elegans* homolog of the Wnt secretory factor *Wntless* (Fig. 2A,B) (Banziger et al., 2006; Bartscherer et al., 2006; Goodman et al., 2006). In the *mig-14*

mutant, Wnt secretion in general is profoundly depleted and very little extracellular Wnt protein is available for signaling. These results are consistent with the model that phenotypic improvement conferred by the *vang-1* mutation depends on the Wnt ligands. Similar to its effects on QL.d, overexpression of VANG-1 in the QR.d caused modest but significant AVM migration defects (Fig. 2A,B). This suggests that *vang-1* antagonizes Wnt signaling in QR.d migration cell-autonomously.

It was previously shown that *mom-5* mutations compromise anterior migration of QR.p neuroblast, whereas *vang-1* mutations move QR.pap (future AVM) further anterior (Mentink et al., 2014). To test whether *vang-1* also plays a role during QR.p migration, we examined the positions of QR.p at a defined developmental time point during its anterior migration in L1 larvae. The V5R seam cell divides after the QR.a and QR.P start their anterior migration. We scored QR.p positions in L1 animals in which the V5R seam cell has divided but the two V5R daughter cells remain in contact (Fig. 2C). This experiment confirmed that the anterior migration of QR.p was compromised in the *mom-5* mutant, and the *vang-1* mutation significantly suppressed the QR.p defects (Fig. 2C,D). These data indicate that *vang-1* antagonizes Wnt signaling during QR.p neuroblast migration.

VANG-1 antagonizes Wnt signaling in the early development of multiple classes of *C. elegans* neurons

Since QL and QR neuroblasts share similar developmental history and functional property, we investigate whether *vang-1* antagonizes Wnt signaling in a completely unrelated neuronal type. The hermaphrodite-specific neurons (HSNs) are bilaterally symmetric serotonergic motor neurons that control egg-laying muscles (Desai et al., 1988). HSNs migrate from the posterior towards the future vulval primordium during embryogenesis under the control of multiple *Wnt* and *Frizzled* genes (Fig. 3A) (Garriga et al., 1993; Pan et al., 2006). Various Wnt pathway mutants, including *egl-20/Wnt, mig-14/Wntless, mig-1/Frizzled, cwn-1; egl-20*

or *mig-1 mom-5* double mutants, showed migration defects of HSNs, which fall short of their wild-type positions near the vulval primordium (Fig. 3B-D). Similar to its effects on AVM migration, the *vang-1* mutation suppressed HSN migration defects in the *egl-20, mig-1* or *cwn-1; egl-20* double mutants (Fig. 3B-D). The suppression effect of the *vang-1* mutation was not seen in the *mig-1 mom-5* double mutant or when secreted Wnts were largely eliminated in the *mig-14* mutant (Fig. 3C,D). Restoration of *vang-1* in the HSNs, using the *unc-86* promoter, completely reversed the suppression on HSN migration defects in the *egl-20; vang-1* double mutant, making the HSN defects similar to those of the *egl-20* mutant (Fig. 3D). This rescue effect was abolished by *vang-1* RNAi, suggesting that the reversal of suppression is the action of functional *vang-1* transcripts rather than impairment of HSN migration by use of the *unc-86* promoter (Fig. 3E). These results confirm that *vang-1* antagonizes Wnt signaling cell-autonomously in HSN migration.

Could *vang-1* antagonize Wnt signaling in developmental contexts other than neuronal migration? To explore this possibility, we examine the ALM, a unipolar touch neuron whose morphology is regulated by Wnts (Hilliard and Bargmann, 2006;Prasad and Clark, 2006; Pan et al., 2008; Zheng et al., 2015). The bilaterally symmetric ALM neurons extend a long neurite to the anterior. In the *mig-14* and *cwn-1; egl-20* double mutants, many ALM neurons grew a single posterior neurite that could reach as far as the lumbar ganglia, and some ALMs showed bipolar morphology with both anterior and posterior neurites (Fig. S3A,B). The *vang-1* mutation partially suppressed ALM defects in the *cwn-1; egl-20*, but not in the *mig-14* mutants (Fig. S3B). Moreover, *vang-1* overexpression in the touch neurons caused ALM defects similar to those seen in the *cwn-1; egl-20* mutants in a dose-dependent manner (Fig. S3C). Considering all data from the QL.d, QR.d, HSN and ALM experiments, we conclude that *vang-1* broadly antagonizes Wnt signaling in multiple events of early neuronal development in *C. elegans*.

vang-1 acts through *arr-1*/*β-arrestin2* to antagonize Wnt signaling in neuronal development

Our genetic analyses of neuronal migration raise a possibility that *vang-1* negatively regulates Wnt signaling at the level of Frizzled receptors. A previous study of growth cone steering suggests that Vangl2 facilitates Frizzled endocytosis by antagonizing Dvl1/Dishevelled-mediated Frizzled hyperphosphorylation (Shafer et al., 2011). We previously found that the localization of MIG-1 to RAB-5(+) early endosomes was decreased in the non-migratory *C. elegans* PLM neuron in the *vang-1* mutant, and VANG-1 overexpression increased MIG-1 distribution to the early endosomes (Chen et al., 2017). On the basis of these observations, we hypothesize that VANG-1 antagonizes Wnt signaling by promoting Frizzled endocytosis, thereby terminating signal transduction induced by binding of Wnt ligands to the Frizzled receptors. This model makes three predictions. First, blocking endocytosis should suppress neuronal migration defects caused by a partial deficiency in Frizzled receptors. Second, suppression of neuronal defects conferred by the *vang-1* mutation is not further enhanced by blocking Frizzled endocytosis. Third, loss of VANG-1 impairs Frizzled endocytosis in the migrating neurons and results in higher Frizzled levels at the plasma membrane.

We tested the first prediction by examining animals that carried a deletion in the *arr-1* gene, which encodes the adaptor protein β-arrestin2 essential for Frizzled endocytosis in mammalian cells (Chen et al., 2003). We recently confirmed that *arr-1* also mediated MIG-1 endocytosis in the non-migratory *C. elegans* PLM neuron (Chen et al., 2017). While the *arr-1* mutation did not affect PVM migration in the wild type, similar to the *vang-1* mutation, it significantly suppressed PVM defects in the *mig-1* mutant (Fig. 4A). Likewise, defective AVM migration in the *mom-5* mutant and HSN undermigration of the *egl-20* mutant were also suppressed by the *arr-1* mutation (Fig. 4B,C). These results suggest that in the migrating *C. elegans* neurons, Frizzled endocytosis negatively regulates Wnt signaling. To test whether *vang-1* acts in the same genetic pathway with *arr-1*, we constructed multiple mutants that

harbored both the *vang-1* and *arr-1* mutations, together with the *mig-1* or the *egl-20* mutation. PVM migration defects in the *mig-1; arr-1 vang-1* triple mutant were comparable to those of the *mig-1; vang-1* or the *mig-1; arr-1* mutants (Fig. 4A). This observation suggests that *arr-1* and *vang-1* act in a shared genetic pathway to temper Wnt-Frizzled signaling in QL.d migration. Consistent with this, HSN undermigration was not further worsened in the *egl-20; arr-1 vang-1* triple mutant, compared to those in the *egl-20; arr-1* or *egl-20; vang-1* double mutant (Fig. 4C).

We further investigate the order of *vang-1* and *arr-1* function by genetic epistasis, taking advantage of the neuronal defects caused by *vang-1* overexpression. PVM and AVM migration defects caused by *vang-1* overexpression were ameliorated in the *arr-1* mutant (Fig. 4A,B). Moreover, the *arr-1* mutation also significantly reduced the ALM polarity defects induced by excess *vang-1* activity (Fig. S3C). These results imply that *arr-1* acts downstream of *vang-1* to antagonize Wnt signaling.

VANG-1 promotes endocytosis of the Frizzled receptors

Our previous work indicates that VANG-1 promotes the endocytosis of MIG-1 in the PLM touch neuron (Chen et al., 2017). Taken with results from the genetic experiments that VANG-1 attenuates Frizzled-dependent Wnt signaling and acts upstream of ARR-1/β-arrestin, we hypothesize that VANG-1 facilitates endocytosis of the Frizzled receptors in the Q.d and other neuronal types. To test this, we investigate whether VANG-1 regulates Frizzled localization in the Q.d. For unknown reason, fluorescence signals from our MIG-1::GFP transgene that fully rescued the PVM defects of the *mig-1* mutant, could not be detected in the migrating QL.d (data not shown). Therefore, we used the previously characterized *mom-5* transgene, *zuIs145(Pnmy-2::MOM-5::GFP)* (Park et al., 2004), and observed MOM-5::GFP distribution with or without *vang-1* in QR.d. Because *zuIs145* seemed to be integrated to the sex chromosome and failed to recombine with the sex chromosome-located *vang-1(tm1422)*

allele, we used the CRISPR-Cas9 method to generate the *vang-1(twn3)* null mutation in the *zuIs145* background (Figs. 5A and S1C). We first confirmed that the *vang-1(twn3)* mutation suppressed PVM migration defects of the *mig-1* mutant to comparable level as by other *vang-1* alleles (Fig. S1C). In the QR.d of the wild type, MOM-5::GFP signals were distributed at the plasma membrane and intracellularly (Fig. 5B). By contrast, in the *vang-1(twn3)* mutant, intracellular MOM-5::GFP signals in QR.d were significantly reduced with reciprocal accumulation of MOM-5::GFP at the cell membrane (Fig. 5B,C). We further confirmed this result by performing *vang-1* RNAi, which resulted in the enrichment of MOM-5::GFP signals at the plasma membrane of QR.d (Fig. S4A,B). Moreover, overexpression of *vang-1* diminished membrane MOM-5::GFP, with reciprocal increase of MOM-5::GFP signals in the cytosol (Fig. 5B,C). An *arr-1* mutation engineered by CRISPR-Cas9 resulted in MOM-5::GFP accumulation at the cell membrane, confirming that these changes in MOM-5::GFP distribution indicate endocytosis blockade (Fig. 5B,C). We verified that the GFP-fused MOM-5 proteins are functional, as *zuIs145* significantly rescued AVM undermigration of the *mom-5* mutants (Fig. S4C). Together these results indicate that VANG-1 mediates MOM-5 endocytosis cell-autonomously.

VANG-1 forms protein complexes with Frizzled receptors

We previously showed that VANG-1 complexed with MIG-1 when expressed in mammalian cells (Chen et al., 2017), and this was again confirmed in the current study (Figs. 6A, 6B and S5A). To investigate whether VANG-1 also forms complexes with MOM-5, we expressed HA-tagged VANG-1 and FLAG-tagged MOM-5 in HEK293 cells. Pull-down of MOM-5 by FLAG antibodies co-immunoprecipitated VANG-1, suggesting that VANG-1 and MOM-5 form protein complexes (Figs. 6A, 6C and S5B). To gain further insight into the interaction between VANG-1 and Frizzled proteins, we generated truncated MIG-1 and MOM-5 proteins that lacked the Wnt-binding, cysteine-rich domain (ΔCRD). Removal of the CRD profoundly

weakened the ability of either MIG-1 or MOM-5 to co-immunoprecipitate VANG-1, whereas deletion of the cytoplasmic domain (ΔC) of MIG-1 had no effects (Figs. 6B, 6C and S5). We were not able to express MOM-5 that lacks the cytoplasmic domain in mammalian cells for unknown reason. These results are consistent with the observation from a prior *Drosophila* study reporting that the Frizzled CRD binds Strabismus/Vangl2 (Wu and Mlodzik, 2008), and indicate that the CRD of Frizzleds is important for VANG-1-Frizzled interaction.

DISCUSSION

In addition to its well-established function in the development of *Drosophila* eye and wing discs, PCP signaling also plays important roles in various aspects of vertebrate neuronal development, such as neural tube closure, polarization of inner hair cells, neuronal migration and axon guidance (Goodrich, 2008; Tissir and Goffinet, 2013;Zou, 2012). In neural tube closure, PCP signaling generates molecular asymmetries within and between neuronal precursors that polarize these cells uniformly along the tissue plane to enable convergent extension, a critical process that elongates the vertebrate embryo. Compared to these early morphogenetic events, our understanding of mechanisms by which PCP signaling controls long-range neuronal migration and axon guidance is rather incomplete. The current study establishes that VANG-1 acts cell-autonomously in migrating *C. elegans* neurons and tempers Wnt signaling by facilitating Frizzled endocytosis. These findings extend current understanding of how PCP signaling controls neuronal development and shapes the connectivity of the nervous system.

VANG-1/Vangl2 shapes Wnt signaling depending on the cellular contexts of the neurons

vang-1, the *C. elegans* Vangl2 homolog, is involved in several morphogenetic events that bear some similarity to *Drosophila* or vertebrate PCP, such as the assembly of ventral nerve cord where immature neurons display transient rosette formation similar to that in vertebrate

convergent extension movement (Shah et al., 2017), or the repositioning of endodermal descendants during intestinal morphogenesis (Asan et al., 2016). *vang-1* also controls neuronal polarization (Sanchez-Alvarez et al., 2011), neurite outgrowth (Zheng et al., 2015) and neurite branching (Chen et al., 2017). Mentink et al. reported that *vang-1* controls the final positions of two QR.d, QR.paa (future AVM) and QR.pap (Mentink et al., 2014). In the *vang-1* mutant, QR.paa and QR.pap are positioned more anteriorly compared to those in the wild type, a phenotype that is opposite to that caused by loss of *egl-20/Wnt*, *cwn-1/Wnt* or *mom-5/Frizzled* (Mentink et al., 2014). This observation is consistent with our model that *vang-1* antagonizes a Wnt signaling cascade composed of *egl-20*, *cwn-1* and *mom-5* in QR.d. These results contrast with those in our prior study, which showed that *vang-1* promotes Wnt signaling to pattern neurite branching in the non-migratory PLM neuron (Chen et al., 2017). Because in both studies evidence suggests that *vang-1* facilitates Frizzled endocytosis, we speculate that cellular contexts determine whether VANG-1-mediated Frizzled internalization upregulates or diminishes Wnt signaling. In immature neurons that undergo long-range migration or cellular polarization, Frizzled internalization terminates Wnt signaling. By contrast, when neurons mature and begin to grow collateral branches in their neurites, as in the case of PLM, Frizzled endocytosis transduces Wnt signaling (Chen et al., 2017). These observations expand the spectrum of Wnt-PCP pathways, implying that VANG-1 directly tunes a Wnt signaling cascade previously thought to be distinct from the PCP pathway, thus blurring the boundaries between the β-catenin and PCP branches of Wnt signaling.

Anterior displacement of QL.d in the *egl-20* mutants has led to the hypothesis that these mutant QL.d have acquired the property of QR.d, which migrate anteriorly. This hypothesis gains some support from the observation that a *cwn-1/Wnt* mutation shifts the positions of QL.d in the *egl-20* mutants towards the posterior, which is explained by the fact that *cwn-1* drives QR.d anterior migration (Zinovyeva et al., 2008). It is therefore intriguing why the migration defects of QR.d, but not those of QL.d, are suppressed by *vang-1* mutations in the

egl-20 mutants. However, QL.d in the *cwn-1; egl-20* sometimes occupies a position that is even more posterior than QL.d in the wild type. The distribution of QL.d in the *cwn-1; egl-20* double mutant is also more posterior compared to that of QR.d in the same mutant (Zinovyeva et al., 2008). These observations suggest that QL.d in the *egl-20* mutants bears some phenotypic similarity to the wild-type QR.d, but their molecular property could still be different. One of these differences is likely the distinct subsets of Frizzled receptors expressed or functioning in QL.d or QR.d. *mig-1* or *lin-17* are required in QL.d, but mutations of these Frizzled genes cause no undermigration or even slight overmigration in QR.d (Zinovyeva et al., 2008; Mentink et al., 2014). On the other hand, *mom-5* is important for QR.d migration yet dispensable for QL.d migration. We speculate that QL.d and QR.d may express different Frizzled receptors, and these Frizzled receptors engage different signaling cascades. All these potentially contribute to the observed difference in QL.d and QR.d regarding their sensitivity to the *vang-1* mutation in the *egl-20* mutant background.

We noted that the distribution of PVM becomes somewhat bimodal when *vang-1* mutations or RNAi are added to the *mig-1* mutant (Figs. 1D, S1A and S1B). It is shown that *egl-20*/Wnt signaling regulates QL lineage migration independent of its distribution (Whangbo and Kenyon, 1999). We speculate that *mab-5* is activated and normal posterior QL.d migration is initiated when Wnt signaling exceeds a threshold in QL.d. Variability in *mab-5* expression increases in the *mig-1* and *lin-17* mutants, and it is proposed that Wnt signaling acts to reduce variability of *mab-5* expression (Ji et al., 2013). We speculate that the *vang-1* mutations restore Wnt signaling intensity in general but do not improve all the regulatory steps within the Wnt signaling network, which in part explains low or no *mab-5* expression in some *mig-1; vang-1* mutant animals and a bimodal distribution of PVM positions.

Genetic and molecular mechanisms by which VANG-1 promotes Frizzled endocytosis

In vertebrate cells, endocytosis of the Frizzled receptors could be mediated by β-arrestin2 or by ZNRF3-dependent ubiquitination (Chen et al., 2003; Koo et al., 2012). While Frizzled endocytosis by ubiquitination clearly downregulates Wnt signaling in both mammalian intestinal epithelium and *C. elegans* neurons (Koo et al., 2012; Moffat et al., 2014), Frizzled internalization by β-arrestin2 could promote Wnt signaling both in vertebrate models of tumorigenesis and *C. elegans* neuronal development (Bonnans et al., 2012; Fereshteh et al., 2012; Seitz et al., 2014; Chen et al., 2017). In the present study, we show that VANG-1 and ARR-1/β-arrestin2 act in a common genetic pathway to internalize Frizzled receptors, and this downregulates Wnt signaling. It remains to be determined whether ZNRF3 and Vangl2-β-arrestin2 cooperate to internalize Frizzleds, or they represent distinct pathways to recycle Frizzleds into separate intracellular compartments. Physical interaction between VANG-1 and Frizzleds requires the Frizzled CRD but not the cytoplasmic domain. One possibility is that binding of VANG-1 to the Frizzled-CRD triggers Frizzled internalization mediated by the β-arrestin2 machinery. A prior study showed that Strabismus, the *Drosophila* Vangl2, binds Frizzled-CRD, and when addressed in the context of epithelial cell polarization, this represents an interaction *in trans* between Frizzleds and Strabismus from neighboring cells (Wu and Mlodzik, 2008). By contrast, our genetic and biochemical data suggest that in *C. elegans* migrating neurons, the interaction between VANG-1 and Frizzled-CRD can occur *in cis*, i.e., in the same cell. While the crystal structure of the Frizzled-8-CRD complexed with the *Xenopus* Wnt-8 ligand had been determined recently (Janda et al., 2012), the structure of Vangl2 or its homologous proteins remains unknown. In the future, it will be important to decipher the structure of Vangl2 by itself and that of Vangl2 complexed with the Frizzled CRD. This will offer critical insight into how binding of diffusible (such as Wnts) or membrane-tethered ligands (such as Vangl2) to the Frizzled-CRD initiates Frizzled endocytosis and tunes Wnt signaling.

Modulation of Wnt signaling that terminates neuronal migration

Wnt signaling had been shown to promote the migration of neurons and growth cones by acting as either attractive or repulsive cues (Yoshikawa et al., 2003; Lyuksyutova et al., 2003; Pan et al., 2006). A recent report in *C. elegans* suggests that signaling through the Frizzled receptor MIG-1 and LIN-17 terminate the anterior migration of QR.paa and QR.pap neurons through the β-catenin BAR-1 (Mentink et al., 2014). Adding to the complexity of Wnt signaling in controlling neuronal migration, Mentink et al. further showed that *vang-1* also acts as a brake to prevent QR.pax to overmigrate. As the migration of QR.p was not affected in the *vang-1* mutant, they concluded that *vang-1* functions independently of Wnt- β-catenin signaling, although no genetic experiments were performed to test the interaction between *vang-1* and the Wnt pathway genes (Mentink et al., 2014). By contrast, we show here that *vang-1* antagonizes Wnt signaling by removing Frizzled receptors from the cell membrane. Since Frizzleds transduce Wnt signaling through both β-catenin-dependent and β-catenin-independent pathways, our results suggest that *vang-1* has a broad, negative impact on Wnt signaling in early neural development. This conclusion is supported by observations made in four different neuronal classes (QL.d, QR.d, HSN and ALM). Unlike QL.d where the target of Wnt signaling for neuronal migration, the Hox gene *mab-5*, had been identified, genes that Wnt-Frizzled signaling targets to promote migration in QR.d and HSN or polarization in ALM remain unknown. Identification of such Wnt target genes in neuronal development helps to clarify the role of *vang-1* in fine-tuning Wnt signaling. Our current study, together with a prior report that PLR-1/ZNRF3 E3 ligase downregulates Wnt signaling by internalizing Frizzleds (Moffat et al., 2014), suggests that timely internalization of Frizzleds is a critical step to prevent aberrant neuronal wiring caused by prolonged Wnt signaling. Understanding the molecular and structural detail of VANG-1-mediated endocytosis of Frizzleds shall offer critical insight into the modulation of Wnt signaling in early neuronal development.

MATERIALS AND METHODS

Key Resources

Key experimental materials, including *C. elegans* and bacterial strains, cell lines or antibodies, are listed in Table S1. *C. elegans* strains were cultured and maintained as described (Brenner, 1974). The HEK293 cell line used in this study is from American Type Culture Collection (ATCC) and is authenticated and tested for contamination. The antibodies used in this study are validated by

Generation of the *vang-1(twn3)* allele by CRISPR-Cas9 gene editing

Germline CRISPR: We did germline CRISPR as previously described with some modifications (Dickinson et al., 2013). In brief, we co-inject into worms the mixture of the following three plasmids: pDD162*(Peft-3::Cas9)*, PU6::*vang-1* sgRNA(GACACGAGGAGTTGCGTT) or PU6::*arr-1* sgRNA(GGTGACTATGTCGACTTGA), and *unc-22* sgRNA (twitcher phenotypes, as a co-CRISPR marker) (Kim et al., 2014). Twitcher F1 transgenics were subjected to T7 endonuclease digestion to identify nucleotide mismatches caused by Cas9-mediated editing. Homozygotes of the *vang-1(twn3)* thus generated were confirmed by DNA sequencing.

Somatic CRISPR: Somatic CRISPR was performed as previously described (Shen et al., 2014). In brief, we co-injected the mixture of the following plasmids: *Pegl-17::Cas9* (Q/V5 lineage-specific), PU6::*vang-1* sgRNA(GACACGAGGAGTTGCGTT) and the co-injection markers *Pgcy-8::mCherry* (for isolation of transformants) and *Pmec-7::mCherry*. To optimize the expression of transgenes, animals are cultivated at 25˚C, and PVM positons are scored with *Pmec-7::mCherry* that label the six touch mechanosensory neurons.

Plasmid construction and molecular biology

We used standard molecular biology techniques to do cloning and construct plasmids. Constructs used for generating transgenes of the *twnEx* series use the pPD95.77 Fire vector as their backbone. The constructs for expression in the HEK293 cells are in the pcDNA, RK5F vector backbone. Information of primers for cloning *vang-1*, *mig-1*, *mom-5* and *rab-5* are available upon request. Germ line transformation by microinjection was performed as described (Mello et al., 1991).

RNA interference by feeding

Feeding RNAi was performed as described (Kamath et al., 2001). In brief, *vang-1* RNAi bacteria was induced by 1mM isopropyl β-D-1-thiogalactopyranoside (IPTG) for 1.5 hours before seeding on NGM plates supplemented with 1 mM IPTG. Gravid hermaphrodites were bleached on RNAi plates and newly hatched L1 larvae were allowed to develop to adult. This procedure was repeated for one more time before gravid hermaphrodites were collected and bleached to obtain synchronized early L1 larvae arrested in M9 buffer. These arrested L1 larvae were then released on fresh *vang-1* RNAi plates and scored at appropriate stages for individual phenotypes (2-3 hours post-hatching L1 for MOM-5::GFP quantification, and late L4 for PVM positions).

Quantification of neuronal positions by epifluorescence microscopy

The transgene *zdIs5(Pmec-4::gfp)* labels PVM and AVM, and integrated array *mgIs42(Ptph-1::gfp)* or extrachromosomal array *twnEx199(Punc-86::gfp)* mark HSN. 1% sodium azide was used to anesthetize the late L4 animals. Neurons were imaged under the 10X objective of the AxioImager M2 imaging system (Carl Zeiss). For quantifying AVM and PVM positions, we set the nose tip as zero and the tail tip as one. AVM and PVM positions are defined as

fractions of the nose-to-tail length. For quantifying HSN positions, we set the vulva opening as zero and the tail tip as one, as normally the HSNs do not migrate anterior to the vulva. HSN positions are defined as fractions of the vulva-to-tail distance. Pixel-wise measurement of length was performed with ImageJ.

Characterization of ALM polarity

The transgene *zdIs5(Pmec-4::gfp)* also labels the ALM and PLM touch receptor neurons. L4 animals were anesthetized with 1% sodium azide as described. Neurons were imaged under the 10X objective of the AxioImager M2 imaging system (Carl Zeiss). Bipolar polarity defect is defined as ALM neurons with the normal anterior process and a posterior process longer than 10 times cell diameter in Wnt pathway mutant and this definition is the same as method in previous method (Pan et al., 2008); in VANG-1 overexpression, bipolar polarity defect is defined as ALM neurons with the normal anterior process and a posterior process longer than 5 times cell diameter. Reversed polarity defect is defined as ALM neurons having a long posterior process without the normal anterior process.

Quantification of *mab-5* expression by fluorescent microscopy

The transgene *muIs16(Pmab-5::gfp)* was used to observe *mab-5* expression, with QL.a and QL.p marked by *rdvIs1(Pegl-17::Myri::mCherry)*. We synchronized early L1 larvae by hatching them in M9 buffer, and scored them after resuming feeding for 2 to 3 hours on regular OP50 *E. coli* plates. L1 larvae were observed by the 100X objective of the AxioImager M2 imaging system (Carl Zeiss) and AxioCam MRm CCD camera (Carl Zeiss) under identical imaging parameters. GFP pixel density OF *muIs16* in QL.d, the boundary of which is defined by *rdvIs1*, was quantified using NIH public software ImageJ.

Characterization of MOM-5::GFP by confocal microscopy

We used *rdvIs1(Pegl-17::Myri::mCherry)* to label the Q cell lineages that highlights the plasma membrane, and *zuIs145(Pnmy-2::mom-5::gfp)* to observe MOM-5::GFP signal (Ou et al., 2010;Park et al., 2004). Note that chromosomes are also labeled by *rdvIs1*. Early L1 larvae (post-hatching 1~2 hours) were examined under the 100X objective of the LSM 700 Confocal System (Carl Zeiss), and series of z-stack projection images were acquired using the Zeiss Zen software under identical parameters. For this analysis we focused on QR.a and QR.p. Pixel-wise quantification for GFP fluorescence intensity was quantified by Image J for individual optical slices, and summation of all optical section from the same z-stack series was represented. To determine the subcellular distribution of MOM-5::GFP, cell membrane MOM-5::GFP signals were first quantified using *rdvIs1* as a reference for QR.d membrane. Cytosolic MOM-5::GFP signals were derived by subtracting membrane MOM-5::GFP signals from total MOM-5::GFP signals.

Co-immunoprecipitation and western blotting

Gene constructs were transfected into HEK293 cells with lipofectamine (Invitrogen) and grown for 2 days before lysis with buffer (50 mM Tris, 150 mM NaCl, 2 mM EDTA pH = 8.0, 0.5% Sodium Deoxylcholate, 10 mM phenylmethylsulfonyl fluoride, 1M Dithiothreitol, 1% NP-40), protease inhibitor cocktail (Roche) and 20 mM sodium fluoride. For co-immunoprecipitation, we used anti-HA (Invitrogen) or anti-FLAG (Sigma) beads to pull down proteins from cell lysates. After proteins (1 μg) bind to the beads, we add 4X sample buffer with 10% β-mercaptoethanol and incubate samples at 37°C for 20 minutes to prevent aggregation of transmembrane proteins. Samples for western blot analysis were electrophoresed in 10% SDS-polyacryalamide gel and transferred onto the PVDF membrane. We used anti-HA, ant-FLAG or anti-β-actin antibodies as described in the Key Resources

Table to detect protein signals.

Statistics

For all samples, n represents the number of cells scored. Cells are excluded only when they cannot be unambiguously identified or visualized. One-way ANOVA followed by Bonferroni's multiple comparison test is used for multiple comparisons between conditions within a dataset. For data in Fig. 2D, Fisher exact test is used. Statistics is performed by Prism.

Data Availability

All data are presented in the paper and there is no deposited data somewhere else.

Acknowledgements

We thank Gian Garriga and the *C. elegans* Genetics Center (CGC) for worm strains. CGC is funded by NIH Office of Research Infrastructure Programs (P40 OD010440). This study was funded by the Ministry of Science and Technology (MOST), Taiwan, to C.L.P. (MOST 103-2320-B-002-050-MY3, MOST 106-2320-B-002-051-MY3).

Competing interests

The authors declare no competing interests.

Author contributions

Conceptualization: C.W.H., C.K.C., C.L.P.; Methodology: C.W.H., C.K.C., C.P.L., J.T., C.H.C., C.L.P.; Validation: Formal Analysis: C.W.H., C.K.C., C.P.L., C.L.P.; Writing - original draft: C.W.H; Writing - review & editing: C.W.H, C.L.P.; Supervision: C.L.P.; Project administration: C.L.P.; Funding: C.L.P.

Reference

Asan, A., Raiders, S. A. & Priess, J. R. (2016). Correction: Morphogenesis of the C. elegans Intestine Involves Axon Guidance Genes. *PLoS Genet,* **12,** e1006077.

Bailly, E., Walton, A. & Borg, J. P. (2017). The Planar Cell Polarity Vangl2 protein: from genetics to cellular and molecular functions. *Semin Cell Dev Biol*.

Banziger, C., Soldini, D., Schutt, C., Zipperlen, P., Hausmann, G. & Basler, K. (2006). Wntless, a conserved membrane protein dedicated to the secretion of Wnt proteins from signaling cells. *Cell,* 125**,** 509-22.

Bartscherer, K., Pelte, N., Ingelfinger, D. & Boutros, M. (2006). Secretion of Wnt ligands requires Evi, a conserved transmembrane protein. *Cell,* **125,** 523-33.

Blockus, H. & Chedotal, A. (2016). Slit-Robo signaling. *Development,* **143,** 3037-44.

Bonnans, C., Flaceliere, M., Grillet, F., Dantec, C., Desvignes, J. P., Pannequin, J., Severac, D., Dubois, E., Bibeau, F., Escriou, V., Crespy, P., Journot, L., Hollande, F. & Joubert, D. (2012). Essential requirement for beta-arrestin2 in mouse intestinal tumors with elevated Wnt signaling. *Proc Natl Acad Sci U S A,* **109,** 3047-52.

Brenner, S. (1974). The genetics of Caenorhabditis elegans. *Genetics,* **77,** 71-94.

Chen, C. H., He, C. W., Liao, C. P. & Pan, C. L. (2017). A Wnt-planar polarity pathway instructs neurite branching by restricting F-actin assembly through endosomal signaling. *PLoS Genet,* **13,** e1006720.

Chen, W., Ten Berge, D., Brown, J., Ahn, S., Hu, L. A., Miller, W. E., Caron, M. G., Barak, L. S., Nusse, R. & Lefkowitz, R. J. (2003). Dishevelled 2 recruits beta-arrestin 2 to mediate Wnt5A-stimulated endocytosis of Frizzled 4. *Science,* **301,** 1391-4.

Clark, S. G., Chisholm, A. D. & Horvitz, H. R. (1993). Control of cell fates in the central body region of C. elegans by the homeobox gene lin-39. *Cell,* **74,** 43-55.

Desai, C., Garriga, G., Mcintire, S. L. & Horvitz, H. R. (1988). A genetic pathway for the development of the Caenorhabditis elegans HSN motor neurons. *Nature,* **336,** 638-46.

Devenport, D. (2014). The cell biology of planar cell polarity. *J Cell Biol,* **207,** 171-9.

Dickinson, D. J., Ward, J. D., Reiner, D. J. & Goldstein, B. (2013). Engineering the Caenorhabditis elegans genome using Cas9-triggered homologous recombination. *Nat Methods,* **10,** 1028-34.

Dudanova, I. & Klein, R. (2013). Integration of guidance cues: parallel signaling and crosstalk. *Trends Neurosci,* **36,** 295-304.

Eisenmann, D. M. & Kim, S. K. (2000). Protruding vulva mutants identify novel loci and Wnt signaling factors that function during Caenorhabditis elegans vulva development. *Genetics,* **156,** 1097-116.

Fereshteh, M., Ito, T., Kovacs, J. J., Zhao, C., Kwon, H. Y., Tornini, V., Konuma, T., Chen, M., Lefkowitz, R. J. & Reya, T. (2012). beta-Arrestin2 mediates the initiation and progression of myeloid leukemia. *Proc Natl Acad Sci U S A,* **109,** 12532-7.

Forrester, W. C., Kim, C. & Garriga, G. (2004). The Caenorhabditis elegans Ror RTK CAM-1 inhibits EGL-20/Wnt signaling in cell migration. *Genetics,* **168,** 1951-62.

Garriga, G., Desai, C. & Horvitz, H. R. (1993). Cell interactions control the direction of outgrowth, branching and fasciculation of the HSN axons of Caenorhabditis elegans. *Development,* **117,** 1071-87.

Goodman, R. M., Thombre, S., Firtina, Z., Gray, D., Betts, D., Roebuck, J., Spana, E. P. & Selva, E. M. (2006). Sprinter: a novel transmembrane protein required for Wg secretion and signaling. *Development,* **133,** 4901-11.

Goodrich, L. V. (2008). The plane facts of PCP in the CNS. *Neuron,* **60,** 9-16.

Harris, J., Honigberg, L., Robinson, N. & Kenyon, C. (1996). Neuronal cell migration in C. elegans: regulation of Hox gene expression and cell position. *Development,* **122,** 3117-31.

Hilliard, M. A. & Bargmann, C. I. (2006). Wnt signals and frizzled activity orient anterior-posterior axon outgrowth in C. elegans. *Dev Cell,* **10,** 379-90.

Janda, C. Y., Waghray, D., Levin, A. M., Thomas, C. & Garcia, K. C. (2012). Structural basis of Wnt recognition by Frizzled. *Science,* **337,** 59-64.

Ji, N., Middelkoop, T. C., Mentink, R. A., Betist, M. C., Tonegawa, S., Mooijman, D., Korswagen, H. C. & Van Oudenaarden, A. (2013). Feedback control of gene expression variability in the Caenorhabditis elegans Wnt pathway. *Cell,* **155,** 869-80.

Jongbloets, B. C. & Pasterkamp, R. J. (2014). Semaphorin signalling during development. *Development,* **141,** 3292-7.

Kamath, R. S., Martinez-Campos, M., Zipperlen, P., Fraser, A. G. & Ahringer, J. (2001). Effectiveness of specific RNA-mediated interference through ingested double-stranded RNA in Caenorhabditis elegans. *Genome Biol,* **2,** RESEARCH0002.

Keleman, K., Rajagopalan, S., Cleppien, D., Teis, D., Paiha, K., Huber, L. A., Technau, G. M. & Dickson, B. J. (2002). Comm sorts robo to control axon guidance at the Drosophila midline. *Cell,* **110,** 415-27.

Kidd, T., Russell, C., Goodman, C. S. & Tear, G. (1998). Dosage-sensitive and complementary functions of roundabout and commissureless control axon crossing of the CNS midline. *Neuron,* **20,** 25-33.

Kim, H., Ishidate, T., Ghanta, K. S., Seth, M., Conte, D., Jr., Shirayama, M. & Mello, C. C. (2014). A co-CRISPR strategy for efficient genome editing in Caenorhabditis elegans. *Genetics,* **197,** 1069-80.

Koo, B. K., Spit, M., Jordens, I., Low, T. Y., Stange, D. E., Van De Wetering, M., Van Es, J. H., Mohammed, S., Heck, A. J., Maurice, M. M. & Clevers, H. (2012). Tumour suppressor RNF43 is a stem-cell E3 ligase that induces endocytosis of Wnt receptors. *Nature,* **488,** 665-9.

Korswagen, H. C. (2002). Canonical and non-canonical Wnt signaling pathways in Caenorhabditis elegans: variations on a common signaling theme. *Bioessays,* **24,** 801-10.

Korswagen, H. C., Herman, M. A. & Clevers, H. C. (2000). Distinct beta-catenins mediate adhesion and signalling functions in C. elegans. *Nature,* **406,** 527-32.

Lyuksyutova, A. I., Lu, C. C., Milanesio, N., King, L. A., Guo, N., Wang, Y., Nathans, J., Tessier-Lavigne, M. & Zou, Y. (2003). Anterior-posterior guidance of commissural axons by Wnt-frizzled signaling. *Science,* **302,** 1984-8.

Maloof, J. N., Whangbo, J., Harris, J. M., Jongeward, G. D. & Kenyon, C. (1999). A Wnt signaling pathway controls hox gene expression and neuroblast migration in C. elegans. *Development,* **126,** 37-49.

Mello, C. C., Kramer, J. M., Stinchcomb, D. & Ambros, V. (1991). Efficient gene transfer in C.elegans: extrachromosomal maintenance and integration of transforming sequences. *EMBO J,* **10,** 3959-70.

Mentink, R. A., Middelkoop, T. C., Rella, L., Ji, N., Tang, C. Y., Betist, M. C., Van Oudenaarden, A. & Korswagen, H. C. (2014). Cell intrinsic modulation of Wnt signaling controls neuroblast migration in C. elegans. *Dev Cell,* **31,** 188-201.

Moffat, L. L., Robinson, R. E., Bakoulis, A. & Clark, S. G. (2014). The conserved transmembrane RING finger protein PLR-1 downregulates Wnt signaling by reducing Frizzled, Ror and Ryk cell-surface levels in C. elegans. *Development,* **141,** 617-28.

Ou, G., Stuurman, N., D'ambrosio, M. & Vale, R. D. (2010). Polarized myosin produces unequal-size daughters during asymmetric cell division. *Science,* **330,** 677-80.

Pan, C. L., Baum, P. D., Gu, M., Jorgensen, E. M., Clark, S. G. & Garriga, G. (2008). C. elegans AP-2 and retromer control Wnt signaling by regulating mig-14/Wntless. *Dev Cell,* **14,** 132-9.

Pan, C. L., Howell, J. E., Clark, S. G., Hilliard, M., Cordes, S., Bargmann, C. I. & Garriga, G. (2006). Multiple Wnts and frizzled receptors regulate anteriorly directed cell and growth cone migrations in Caenorhabditis elegans. *Dev Cell,* **10,** 367-77.

Park, F. D., Tenlen, J. R. & Priess, J. R. (2004). C. elegans MOM-5/frizzled functions in MOM-2/Wnt-independent cell polarity and is localized asymmetrically prior to cell division. *Curr Biol,* **14,** 2252-8.

Prasad, B. C. & Clark, S. G. (2006). Wnt signaling establishes anteroposterior neuronal polarity and requires retromer in C. elegans. *Development,* **133,** 1757-66.

Sanchez-Alvarez, L., Visanuvimol, J., Mcewan, A., Su, A., Imai, J. H. & Colavita, A. (2011). VANG-1 and PRKL-1 cooperate to negatively regulate neurite formation in Caenorhabditis elegans. *PLoS Genet,* **7,** e1002257.

Seitz, K., Dursch, V., Harnos, J., Bryja, V., Gentzel, M. & Schambony, A. (2014). beta-Arrestin interacts with the beta/gamma subunits of trimeric G-proteins and dishevelled in the Wnt/Ca(2+) pathway in xenopus gastrulation. *PLoS One,* **9,** e87132.

Shafer, B., Onishi, K., Lo, C., Colakoglu, G. & Zou, Y. (2011). Vangl2 promotes Wnt/planar cell polarity-like signaling by antagonizing Dvl1-mediated feedback inhibition in growth cone guidance. *Dev Cell,* **20,** 177-91.

Shah, P. K., Tanner, M. R., Kovacevic, I., Rankin, A., Marshall, T. E., Noblett, N., Tran, N. N., Roenspies, T., Hung, J., Chen, Z., Slatculescu, C., Perkins, T. J., Bao, Z. & Colavita, A. (2017). PCP and SAX-3/Robo Pathways Cooperate to Regulate Convergent Extension-Based Nerve Cord Assembly in C. elegans. *Dev Cell,* **41,** 195-203 e3.

Shen, Z., Zhang, X., Chai, Y., Zhu, Z., Yi, P., Feng, G., Li, W. & Ou, G. (2014). Conditional knockouts generated by engineered CRISPR-Cas9 endonuclease reveal the roles of coronin in C. elegans neural development. *Dev Cell,* **30,** 625-36.

Sun, K. L. W., Correia, J. P. & Kennedy, T. E. (2011). Netrins: versatile extracellular cues with diverse functions. *Development,* **138,** 2153-2169.

Tear, G., Harris, R., Sutaria, S., Kilomanski, K., Goodman, C. S. & Seeger, M. A. (1996). commissureless controls growth cone guidance across the CNS midline in Drosophila and encodes a novel membrane protein. *Neuron,* **16,** 501-14.

Tessier-Lavigne, M. & Goodman, C. S. (1996). The Molecular Biology of Axon Guidance. *Science,* **274,** 1123.

Tissir, F. & Goffinet, A. M. (2013). Shaping the nervous system: role of the core planar cell polarity genes. *Nat Rev Neurosci,* **14,** 525-35.

Wang, B. B., Muller-Immergluck, M. M., Austin, J., Robinson, N. T., Chisholm, A. & Kenyon, C. (1993). A homeotic gene cluster patterns the anteroposterior body axis of C. elegans. *Cell,* **74,** 29-42.

Whangbo, J. & Kenyon, C. (1999). A Wnt signaling system that specifies two patterns of cell migration in C. elegans. *Mol Cell,* **4,** 851-8.

Wu, J. & Mlodzik, M. (2008). The frizzled extracellular domain is a ligand for Van Gogh/Stbm during nonautonomous planar cell polarity signaling. *Dev Cell,* **15,** 462-9.

Yam, P. T. & Charron, F. (2013). Signaling mechanisms of non-conventional axon guidance cues: the Shh, BMP and Wnt morphogens. *Curr Opin Neurobiol,* **23,** 965-73.

Yoshikawa, S., Mckinnon, R. D., Kokel, M. & Thomas, J. B. (2003). Wnt-mediated axon guidance via the Drosophila Derailed receptor. *Nature,* **422,** 583-8.

Zheng, C., Diaz-Cuadros, M. & Chalfie, M. (2015). Dishevelled attenuates the repelling activity of Wnt signaling during neurite outgrowth in Caenorhabditis elegans. *Proc Natl Acad Sci U S A,* **112,** 13243-8.

Zinovyeva, A. Y., Yamamoto, Y., Sawa, H. & Forrester, W. C. (2008). Complex network of Wnt signaling regulates neuronal migrations during Caenorhabditis elegans development. *Genetics,* **179,** 1357-71.

Zou, Y. (2012). Does planar cell polarity signaling steer growth cones? *Curr Top Dev Biol,* **101,** 141-60.

Figures

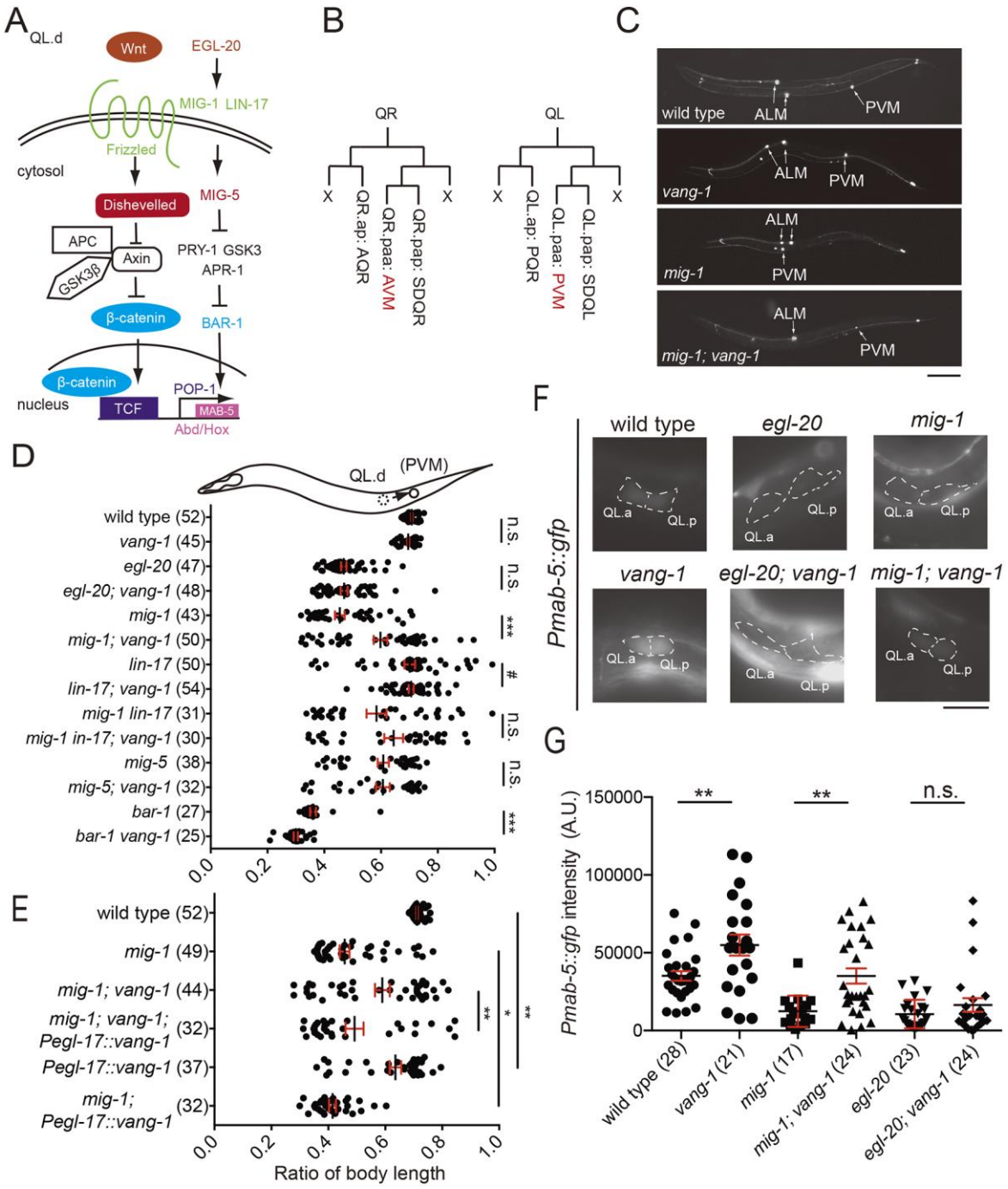

Fig. 1. *vang-1* antagonizes Wnt-Frizzled signaling in the migration of QL.d in *C. elegans*. (A) Schematic diagram of the Wnt signaling pathway that promotes posterior migration of QL.d. (B) Schematic diagram of the Q neuroblast lineages (C) Representative epifluorescent images of PVM neurons in the wild type and the mutants. Scale bar = 100 μm. (D,E) Quantification of PVM positions along the anterior-posterior axis of the worm body. Each dot represents a single PVM neuron, with mean and standard errors of mean (S.E.M.) indicated. N = neurons scored. *, $p < 0.05$, **, $p < 0.01$, ***, $p < 0.001$; one-way ANOVA followed by Bonferroni's multiple comparison test. #, $p < 0.01$; one-way ANOVA followed by Bonferroni's multiple comparison test; see Fig. S2. (F) Epifluorescent images of *Pmab-5::GFP* expression in QL.d of the wild type and the mutants. Dotted lines indicate QL.d in the GFP channel. Scale bar = 10 μm. (G) Quantification of *Pmab-5::GFP* expression. N = number of QL.d scored. **, $p < 0.01$, n.s., not significant; one-way ANOVA followed by Bonferroni's multiple comparison test.

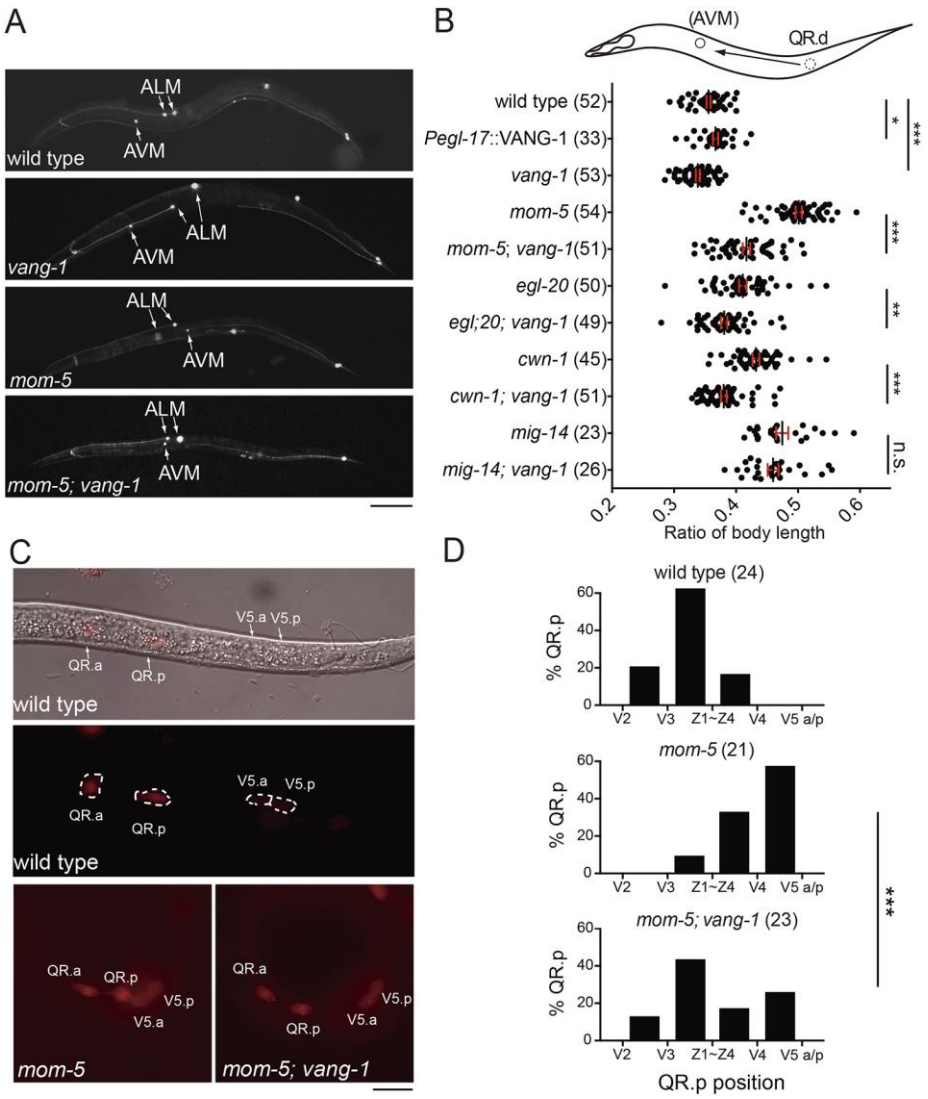

Fig. 2. *vang-1* antagonizes Wnt-Frizzled signaling in the migration of QR.d in *C. elegans*. (A) Representative epifluorescent images of AVM neurons in the wild type and the mutants. The touch neurons are marked by *zdIs5(Pmec-4::GFP)*. Scale bar = 100 µm. (B) Quantification of AVM positions along the anterior-posterior axis of the worm body. Each dot represents a single AVM neuron, with mean and S.E.M. indicated. N = neurons scored. *, $p < 0.05$, **, $p < 0.01$, ***, $p < 0.001$, n.s., not significant; one-way ANOVA followed by Bonferroni's multiple comparison test. (C) Epifluorescent/DIC (top) or epifluorescent images of QR.d in L1 larvae. The Q lineages are labeled by *rdvIs1(Pegl-17::Myri::mCherry).* Scale bar = 10 µm. (D) Distribution of QR.p in L1 at the time of V5R division. ***, $p < 0.001$, Fisher exact test.

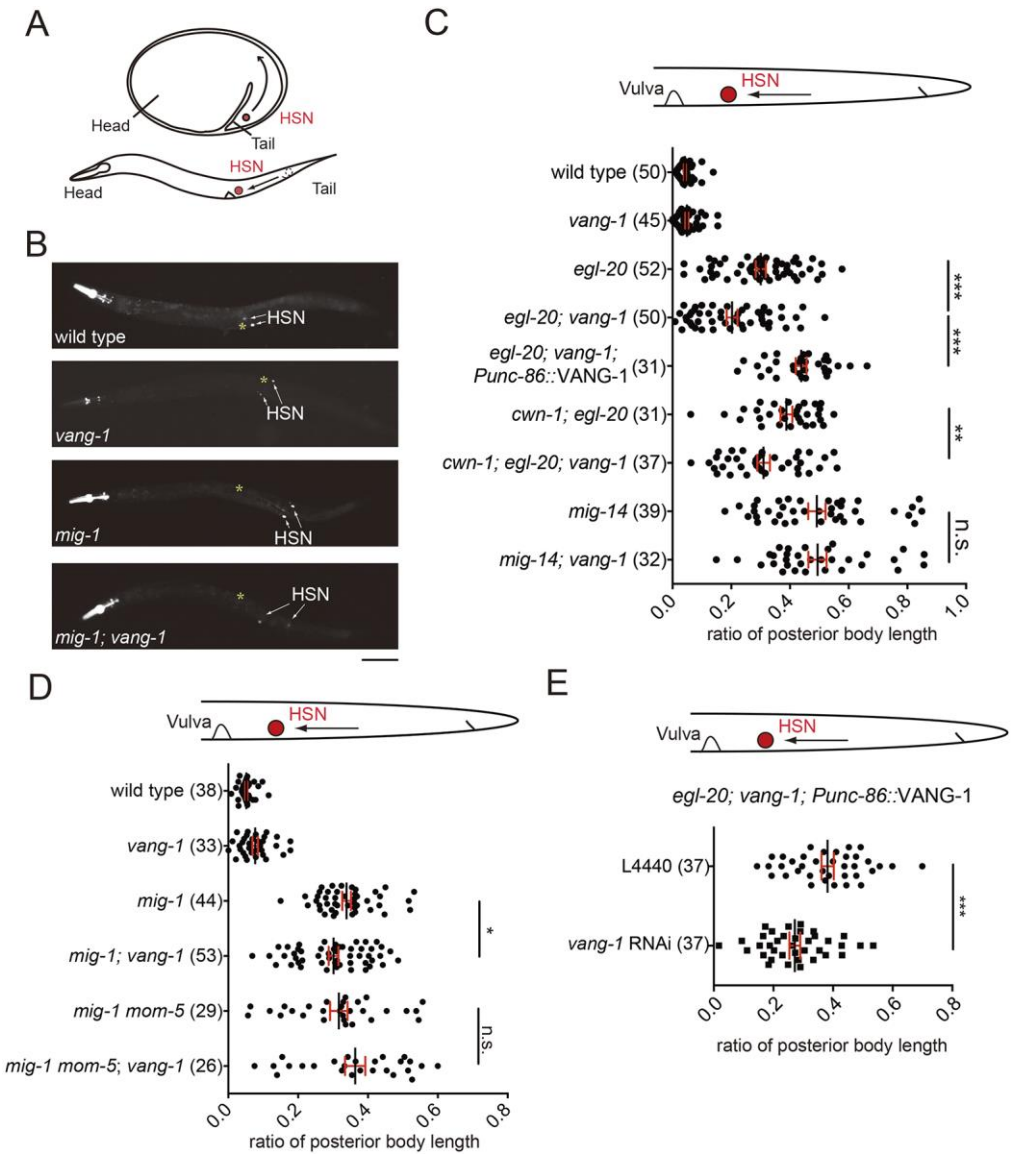

Fig. 3. *vang-1* antagonizes Wnt-Frizzled signaling in the migration of HSN in *C. elegans*. (A) Schematic diagram of HSN migration during embryogenesis and projection of its migratory path onto a late L4 larvae. (B) Representative epifluorescent images of HSN neurons in the wild type and the mutants. Asterisks indicate the position of the vulva. Scale bar = 100 µm. (C,D) Quantification of HSN positions along the anterior-posterior axis of the posterior worm body. Each dot represents a single HSN neuron, with mean and S.E.M. indicated. N = neurons scored. *, $p < 0.05$, **, $p < 0.01$, n.s., not significant; one-way ANOVA followed by Bonferroni's multiple comparison test.

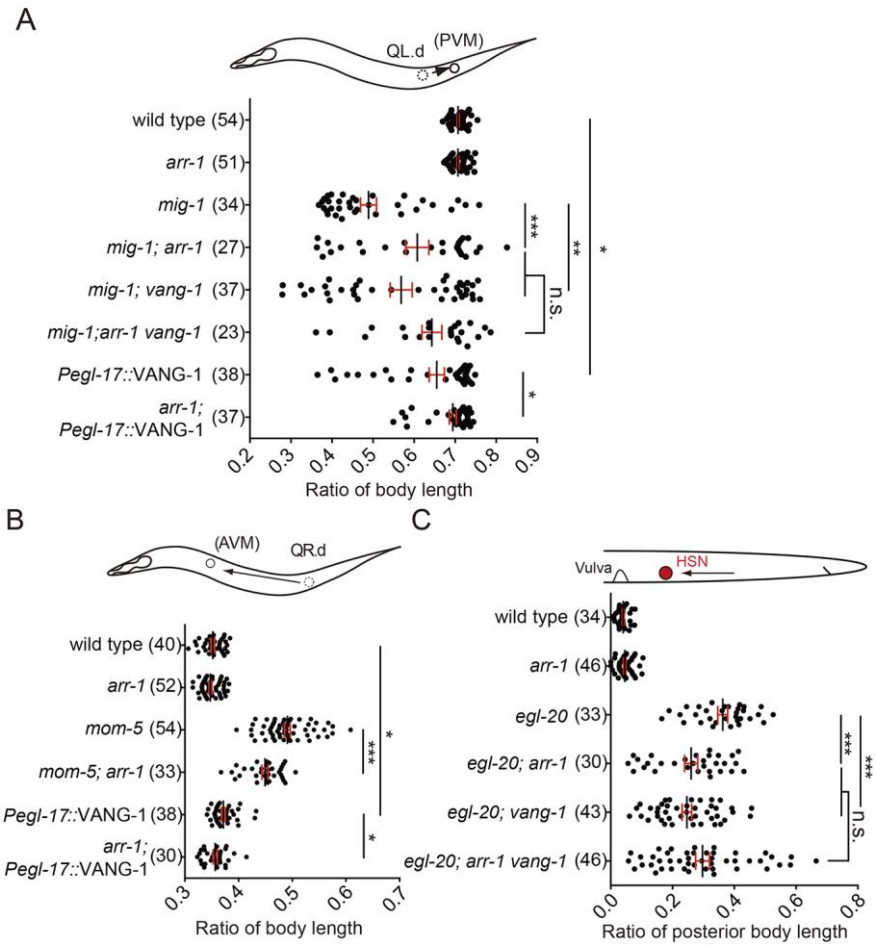

Fig. 4. *vang-1* acts with *arr-1*/β-arrestin2 in the endocytic pathway to antagonize Wnt-Frizzled signaling in neuronal migration. Quantification of the positions of PVM (A), AVM (B) and HSN (C) in the wild type and mutant or transgenic strains. Each dot represents a single neuron, with mean and S.E.M. indicated. N = neurons scored. *, $p < 0.05$, **, $p < 0.01$, ***, $p < 0.001$, n.s., not significant; one-way ANOVA followed by Bonferroni's multiple comparison test.

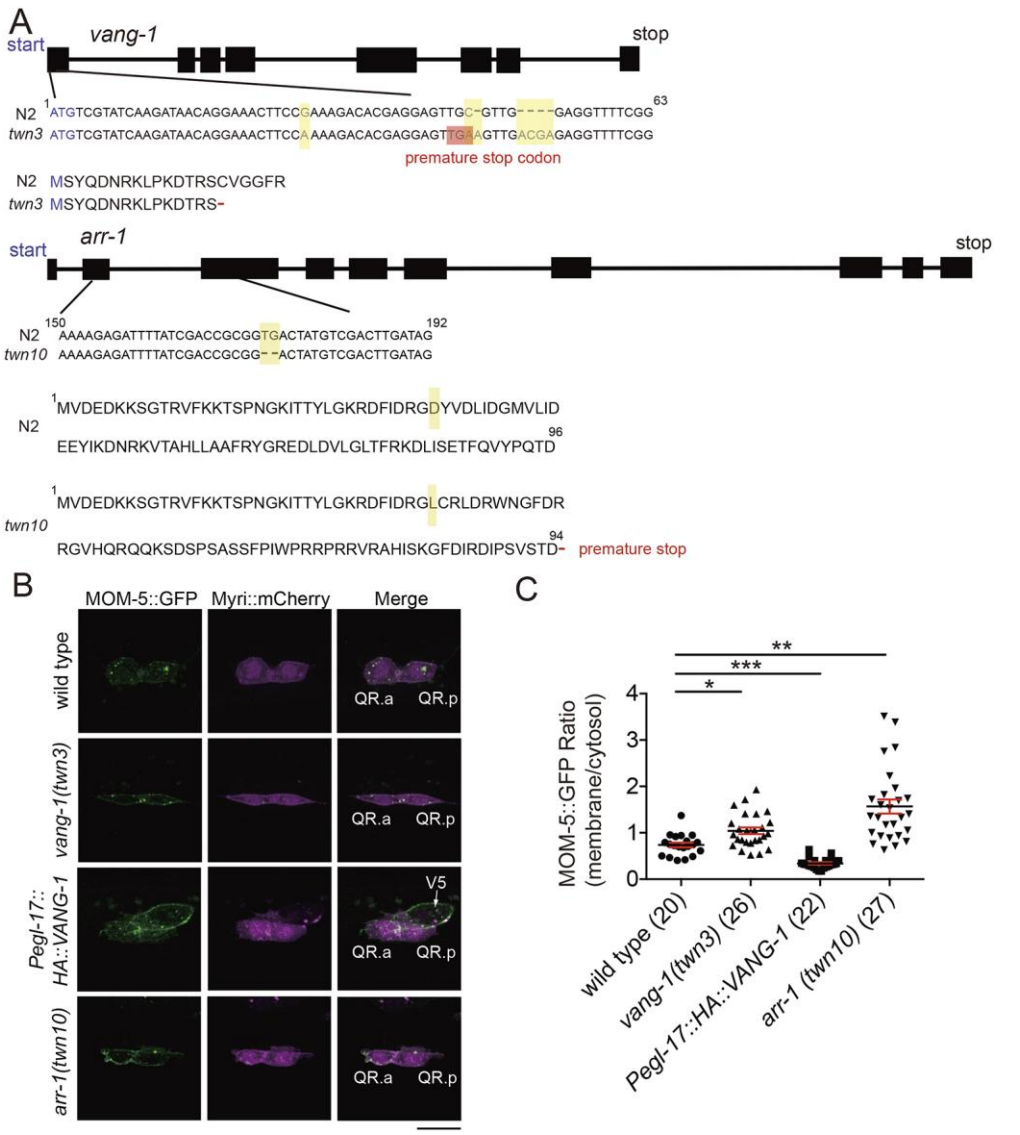

Fig. 5. VANG-1 regulates the distribution of MOM-5 Frizzled receptors on the neuronal membrane. (A) Schematic diagram of the *vang-1(twn3)* and *arr-1(twn10)* mutations engineered by CRISPR-Cas9 into the *zuIs145(Pnmy-2::MOM-5::GFP)* strain. Yellow highlights the changes in the *vang-1(twn3)* and *arr-1(twn10)* alleles. (B, C) Confocal projection images (B) and quantification of MOM-5::GFP distribution (C) in QR.d. MOM-5::GFP is from *zuIs145(Pnmy-2::MOM-5::GFP)* and the QR.d membrane marker is *rdvIs1(Pegl-17::Myri::mCherry)* with mCherry pseudocolored in magenta. The V5R seam cell is indicated. Scale bar = 10 µm. Each dot represents a single neuron, with mean and S.E.M. indicated. N = neurons scored. *, $p < 0.05$, ***, $p < 0.001$; one-way ANOVA followed by Bonferroni's multiple comparison test.

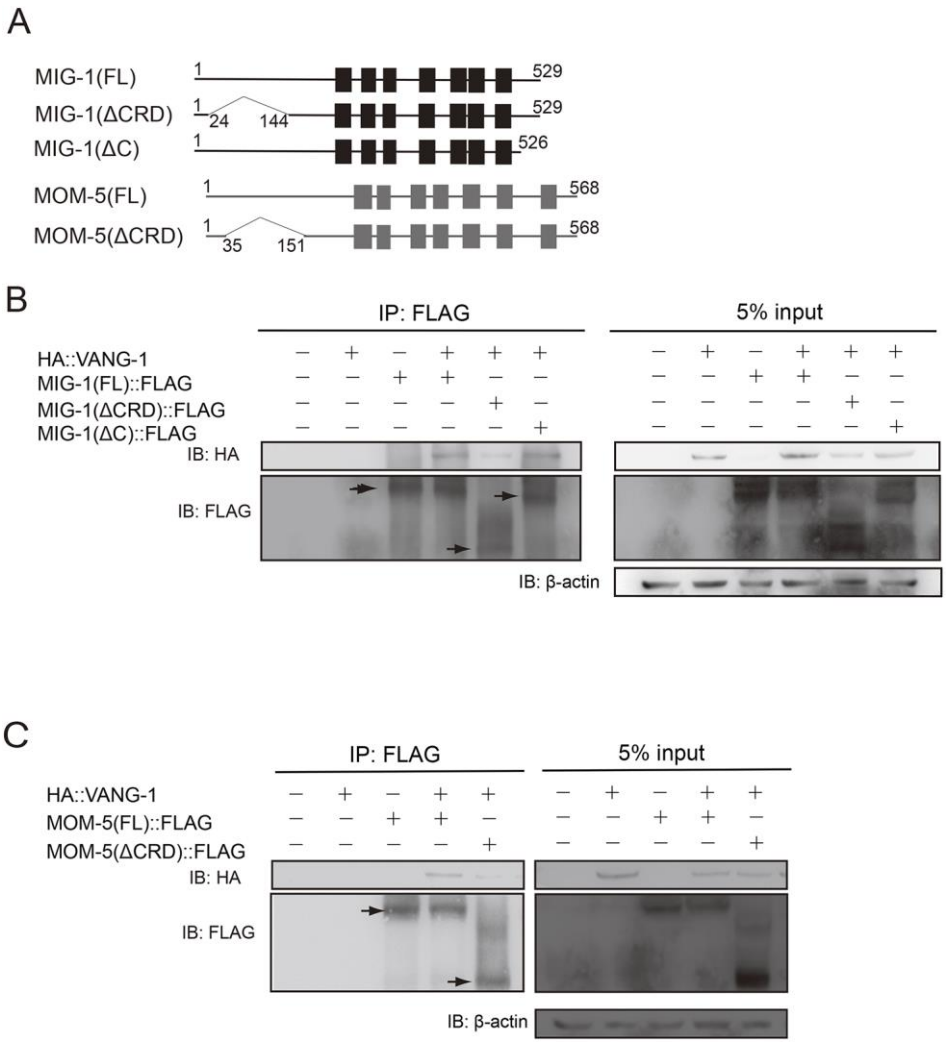

Fig. 6. VANG-1 forms protein complexes with Frizzleds that require the cysteine-rich domains. (A) Schematic diagram of various MIG-1 and MOM-5 deletion mutants used in the co-immunoprecipitation experiments. Filled boxes are transmembrane domains. FL, full-length. (B,C) Co-immunoprecipitation experiments of MIG-1 (B) or MOM-5 (C). Arrows indicate MIG-1 and MOM-5 signals in respective immunoblots.

Table S1. *C. elegans* and bacterial strains, cell lines and antibodies used in the current study.

REAGENT or RESOURCE	SOURCE	IDENTIFIER
Bacterial Strains		
E. coli: Strain OP50	*Caenorhabditis Genetics Center (CGC)*	WormBase: OP50
Chemicals and Antibodies		
Antibody: anti-HA	Abcam	Abcam ab71113 (Duval et al., 2014)
Antibody: anti-FLAG	Sigma	Sigma F7425 (Lee et al., 2014)
Antibody: anti-β-actin	Santa Cruz	Santa Cruz sc- 47778 (Moloughney et al., 2018)
Experimental Models: Cell Lines		
HEK293	ATCC	ATCC: CRL-1573
Experimental Models: Organisms/Strains		
C. elegans: Strain N2: wild isolate	CGC	WormBase: N2
C. elegans: Strain CB3303: *mig-1(e1787) I*	CGC	WormBase: CB3303
C. elegans: Strain MT1306: *lin-17(n671) I*	CGC	WormBase: MT1306
C. elegans: Strain *mom-5(ne12) I*	lab of Craig Mello	N/A
C. elegans: Strain EW12: *mig-14(ga62) II*	CGC	WormBase: EW12
C. elegans: Strain RB763: *cwn-1(ok546) II*	CGC	WormBase: RB763
C. elegans: Strain SU352: *mig-5(rh147) II*	CGC	WormBase: SU352
C. elegans: Strain MT1215: *egl-20(n585) IV*	CGC	WormBase: MT1215

C. elegans: Strain *vang-1(tm1422)X*	Gian Garriga	N/A
C. elegans: Strain *vang-1(twn3)X*	This paper	N/A
C. elegans: Strain RB1125: *vang-1(ok1142) X*	CGC	WormBase:RB1125
C. elegans: Strain EW15: *bar-1(ga80) X*	CGC	WormBase:EW15
C. elegans: Strain RB660: *arr-1(ok401) X*	CGC	WormBase:RB660
C. elegans: Strain SK1006: *zdIs5[Pmec-4::GFP] I*	CGC	WormBase:SK1006
C. elegans: Strain CF453: *muIs16[mab-5::GFP + dpy-20(+)]II; dpy-20(e1282)IV*	CGC	WormBase:CF453
C. elegans: Strain RDV55: *rdvIs1v [Pegl-17::Myri-mCherry::pie-1 3'UTR + Pegl-17::mig-10::YFP::unc-54 3'UTR + Pegl-17::mCherry-TEV-S::his-24 + rol-6(su1006)]III*	CGC	WormBase:RDV55
C. elegans: Strain GR1366: *mgIs42[Ptph-1::GFP + pRF4(rol-6(su1006))]*	CGC	WormBase:GR1366
C. elegans: Strain JJ1992: *zuIs145[unc-119(+) +Pnmy-2::MOM-5::GFP]*	CGC	WormBase:JJ1992
C. elegans: Strain NG4978: *zdIs5; vang-1(tm1422)*	Gian Garriga	N/A
C. elegans: Strain NG6175: *zdIs5; arr-1(ok401)*	Gian Garriga/Jerome	N/A
C. elegans: Strain NG6407: *zdIs5 mig-1(e1787); arr-1(ok401)*	Gian Garriga/Jerome	N/A
C. elegans: Strain CLP293: *muIs16; rdvIs1*	This paper	N/A
C. elegans: Strain CLP392: *zdIs5; mig-5(rh147)*	This paper	N/A
C. elegans: Strain CLP463: *zdIs5; egl-20(n585); vang-1(tm1422)*	This paper	N/A

C. elegans: Strain CLP475: *zdIs5; bar-1(ga80) vang-1(tm1422)*	This paper	N/A
C. elegans: Strain CLP504: *zdIs5; cwn-1(ok546); rdvIs1; vang-1(tm1422)*	This paper	N/A
C. elegans: Strain CLP540: *muIs16; rdvIs1; vang-1(tm1422)*	This paper	N/A
C. elegans: Strain CLP570: *mig-1(e1787); muIs16; rdvIs1; vang-1(tm1422)*	This paper	N/A
C. elegans: Strain CLP571: *muIs16; rdvIs1; egl-20(n585)*	This paper	N/A
C. elegans: Strain CLP580: *muIs16; rdvIs1; egl-20(n585); vang-1(tm1422)*	This paper	N/A
C. elegans: Strain CLP598: *zdIs5 mom-5(ne12)/hT2*	This paper	N/A
C. elegans: Strain CLP605: *zdIs5 mom-5(ne12)/hT2; vang-1(tm1422)*	This paper	N/A
C. elegans: Strain CLP607: *zdIs5; bar-1(ga80)*	This paper	N/A
C. elegans: Strain CLP652: *zdIs5; twnEx230[Pmec-7::gfp::vang-1, Pdpy-30::NLS::DsRed]*	This paper	N/A
C. elegans: Strain CLP702: *zdIs5 mom-5(ne12)/hT2; zuIs145*	This paper	N/A
C. elegans: Strain CLP721: *vang-1(tm1422); mgIs42*	This paper	N/A
C. elegans: Strain CLP734: *zdIs5 mom-5(ne12)/hT2; rdvIs1*	This paper	N/A
C. elegans: Strain CLP737: *zdIs5 mom-5(ne12)/hT2; rdvIs1; vang-1(tm1422)*	This paper	N/A
C. elegans: Strain CLP853: *zdIs5 mig-1(e1787) mom-5(ne12); twnEx199[Punc-86::gfp, Pttx-3::gfp]*	This paper	N/A
C. elegans: Strain CLP863: *zdIs5; mig-5(rh147)/mInI; vang-1(tm1422)*	This paper	N/A

C. elegans: Strain CLP867: *zdIs5 mig-1(e1787); vang-1(ok1142)*	This paper	N/A
C. elegans: Strain CLP870: *zdIs5 mig-1(e1787); twnEx173[Pegl-17::gfp::vang-1, Pgcy-8::mcherry]*	This paper	N/A
C. elegans: Strain CLP871: *zdIs5; twnEx173[Pegl-17::gfp::vang-1, Pgcy-8::mcherry]*	This paper	N/A
C. elegans: Strain CLP872: *zdIs5; arr-1(ok401); twnEx173[Pegl-17::gfp::vang-1, Pgcy-8::mcherry]*	This paper	N/A
C. elegans: Strain CLP874: *zdIs5; mig-14(ga62); vang-1(tm1422); mgIs42*	This paper	N/A
C. elegans: Strain CLP875: zdIs5 mig-1(e1787) mom-5(ne12); vang-1(tm1422); twnEx199[Punc-86::gfp, Pttx-3::gfp]	This paper	N/A
C. elegans: Strain CLP876: *arr-1(ok401); mgIs42*	This paper	N/A
C. elegans: Strain CLP877: egl-20(n585)*; vang-1(tm1422); mgIs42; twnEX340[Punc-86::gfp::vang-1]*	This paper	N/A
C. elegans: Strain CLP878: zdIs5; *twnEx341[Pmec-7::gfp, Pdpy-30::NLS::dsRed](10ng)*	This paper	N/A
C. elegans: Strain CLP879: zdIs5; *twnEx342[Pmec-7::gfp, Pdpy-30::NLS::dsRed]*	This paper	N/A
C. elegans: Strain CLP930: *zdIs5; cwn-1(ok546)*	This paper	N/A
C. elegans: Strain CLP996: *egl-20(n585); mgIs42*	This paper	N/A
C. elegans: Strain CLP999: *mig-1(e1787); vang-1(tm1422); mgIs42*	This paper	N/A
C. elegans: Strain CLP1000: *mig-1(e1787); mgIs42*	This paper	N/A
C. elegans: Strain CLP1004: *egl-20(n585); arr-1(ok401) vang-1(tm1422); mgIs42*	This paper	N/A

C. elegans: Strain CLP1005: *egl-20(n585); arr-1(ok401); mgIs42*	This paper	N/A
C. elegans: Strain CLP1018: *cwn-1(ok546); egl-20(n585); vang-1(tm1422); mgIs42*	This paper	N/A
C. elegans: Strain CLP1021: zdIs5 mig-1(e1787); arr-1(ok401) vang-1(tm1422)	This paper	N/A
C. elegans: Strain CLP1025: *zdIs5; egl-20(n585); arr-1(ok401); mgIs42*	This paper	N/A
C. elegans: Strain CLP1041: *rdvIs1; zuIs145*	This paper	N/A
C. elegans: Strain CLP1043: *cwn-1(ok546); egl-20(n585); mgIs42*	This paper	N/A
C. elegans: Strain CLP1063: *zdIs5 mig-1(e1787) lin-17(n671)*	This paper	N/A
C. elegans: Strain CLP1064: *zdIs5 mom-5(ne12)/hT2; arr-1(ok401)*	This paper	N/A
C. elegans: Strain CLP1065: *mig-1(e1787); muIs16; rdvIs1*	This paper	N/A
C. elegans: Strain CLP1079: *zdIs5 mig-1(e1787) lin-17(n671); vang-1(tm1422)*	This paper	N/A
C. elegans: Strain CLP1081: *zdIs5 mig-1(e1787); twnEx464[Pegl-17::Cas9, Pu6::vang-1(sgRNA)]*	This paper	N/A
C. elegans: Strain CLP1082: *zdIs5 lin-17(n671)*	This paper	N/A
C. elegans: Strain CLP1089: *zdIs5 lin-17(n671); vang-1(tm1422)*	This paper	N/A
C. elegans: Strain CLP1096: *zdIs5 mig-1(e1787); rdvIs1; vang-1(twn3) zuIs145*	This paper	N/A

C. elegans: Strain CLP1100: *rdvIs1; zuIs145; twnEX482[Pegl-17::HA::VANG-1::SL2::BFP]*	This paper	N/A
C. elegans: Strain CLP1120: *rdvIs1; vang-1(twn3) zuIs145*	This paper	N/A
C. elegans: Strain CLP1163: *rdvIs1; arr-1(twn10) zuIs145*	This paper	N/A

Reference

Duval, N., Daubas, P., Bourcier De Carbon, C., St Cloment, C., Tinevez, J. Y., Lopes, M., Ribes, V. & Robert, B. (2014). Msx1 and Msx2 act as essential activators of Atoh1 expression in the murine spinal cord. *Development,* **141,** 1726-36.

Lee, J. H., Daugharthy, E. R., Scheiman, J., Kalhor, R., Yang, J. L., Ferrante, T. C., Terry, R., Jeanty, S. S., Li, C., Amamoto, R., Peters, D. T., Turczyk, B. M., Marblestone, A. H., Inverso, S. A., Bernard, A., Mali, P., Rios, X., Aach, J. & Church, G. M. (2014). Highly multiplexed subcellular RNA sequencing in situ. *Science,* **343,** 1360-3.

Moloughney, J. G., Vega-Cotto, N. M., Liu, S., Patel, C., Kim, P. K., Wu, C. C., Albaciete, D., Magaway, C., Chang, A., Rajput, S., Su, X., Werlen, G. & Jacinto, E. (2018). mTORC2 modulates the amplitude and duration of GFAT1 Ser243 phosphorylation to maintain flux through the hexosamine pathway during starvation. *J Biol Chem*, **293,** 16464-16478.

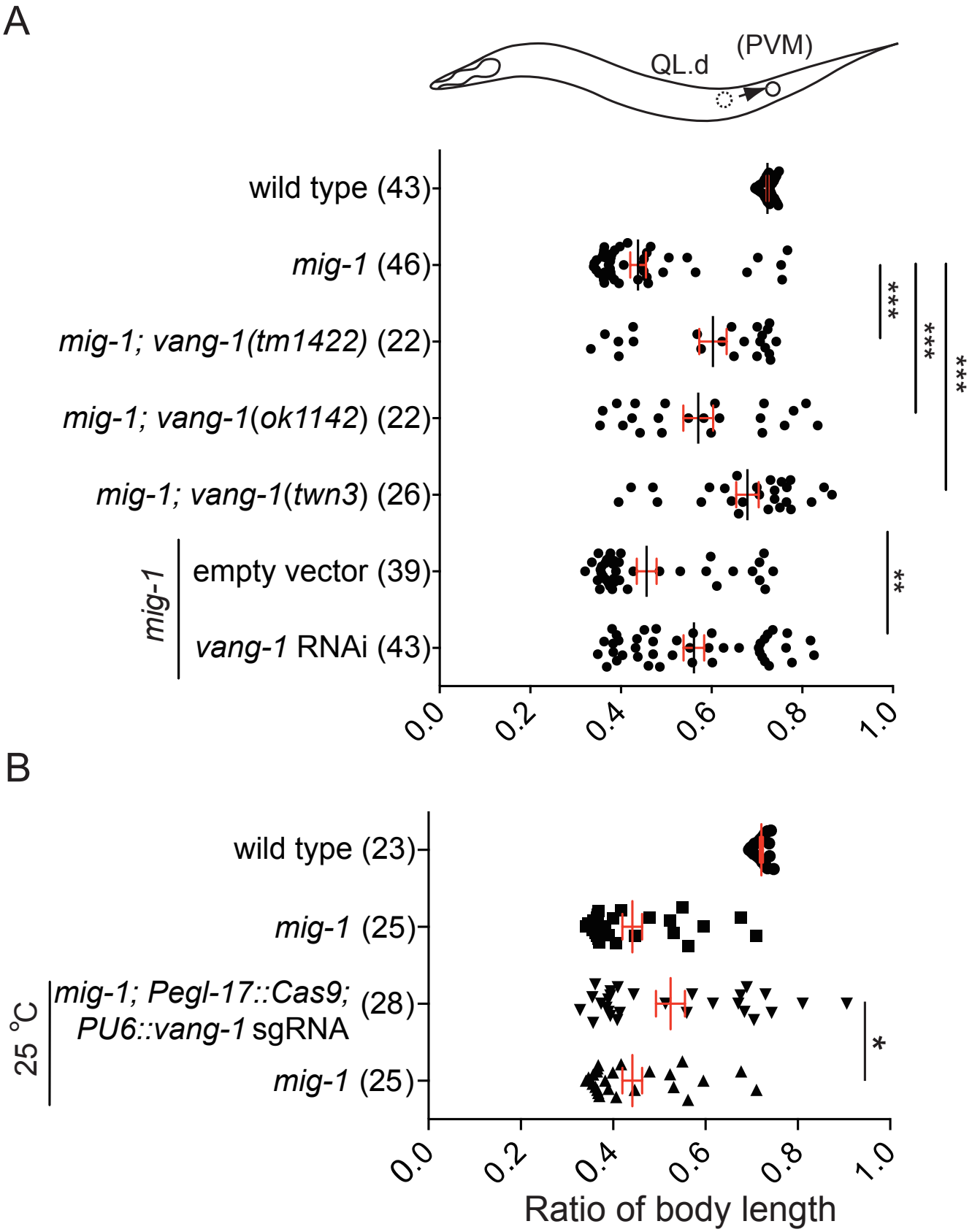

Fig. S1. *vang-1* antagonizes *mig-1* signaling in the migration of QL.d in *C. elegans*.

(A, B) Quantification of PVM positions along the anterior-posterior axis of the worm body. Each dot represents a single PVM neuron, with mean and standard errors of mean (S.E.M.) indicated. N = neurons scored. *, $p < 0.05$, **, $p < 0.01$, ***, $p < 0.001$; one-way ANOVA followed by Bonferroni's multiple comparison test.

A

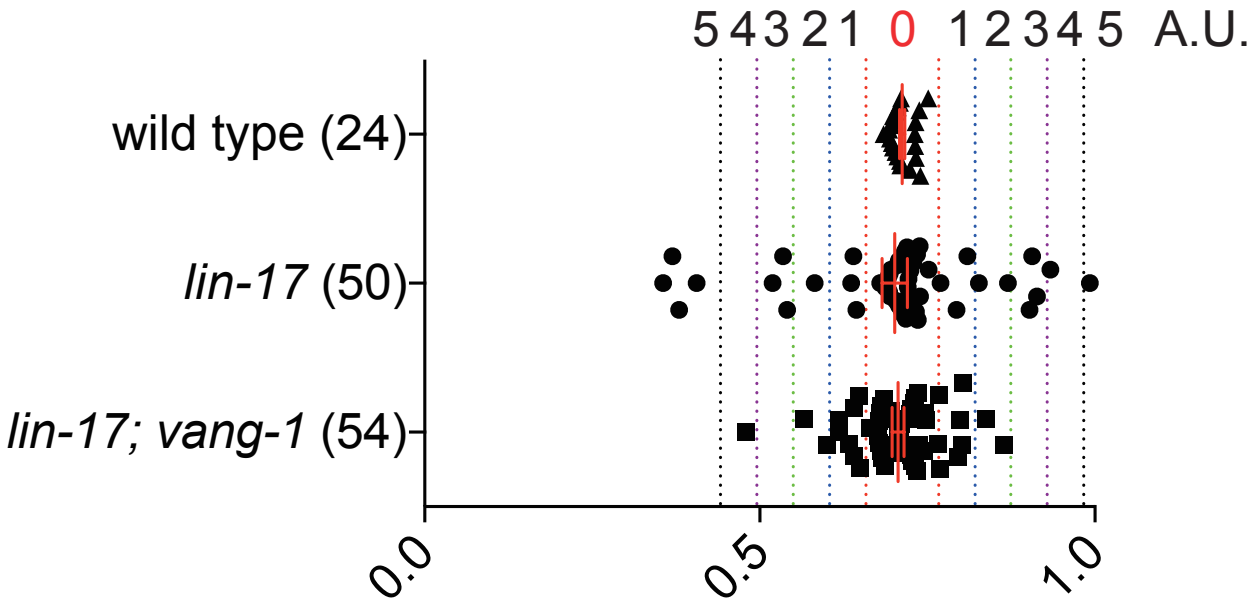

B

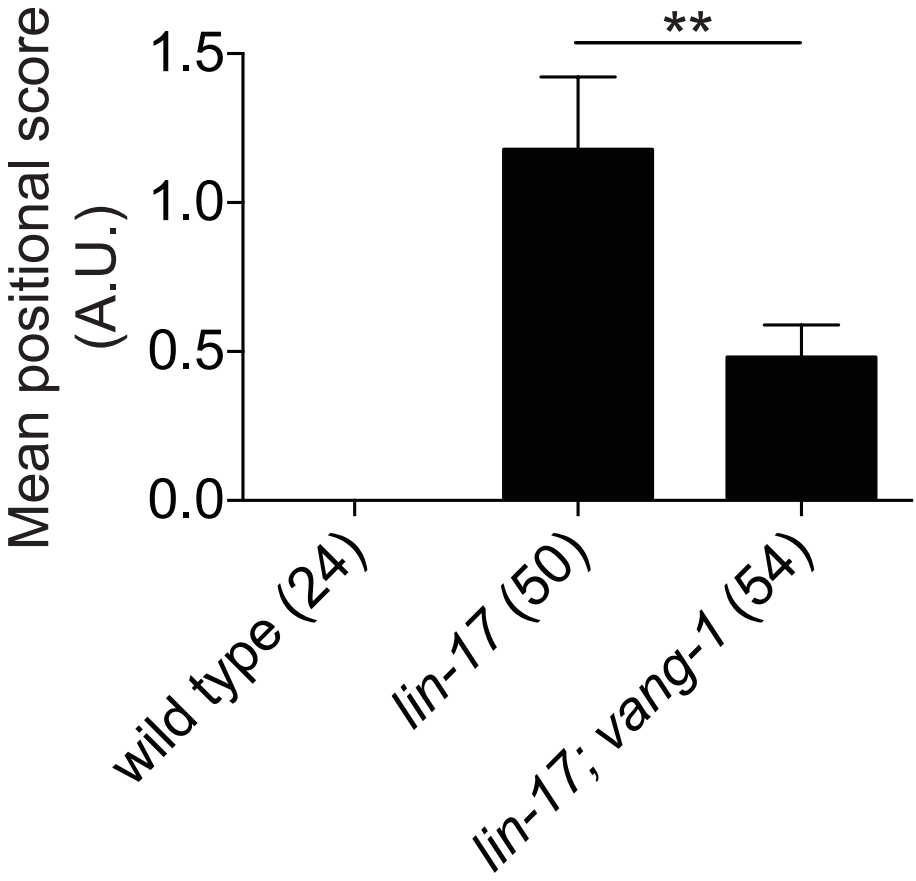

Fig. S2. *vang-1* antagonizes *lin-17* signaling in the migration of QL.d in *C. elegans*. (A) Quantification of PVM positions along the anterior-posterior axis of the worm body. Each dot represents a single PVM neuron, with mean and standard errors of mean (S.E.M.) indicated. N = neurons scored. PVM positions are quantified based on their deviation from the wild-type zone (defined by the red dotted lines, mean ± 3 S.D.) Each zone represents a distance of 3-S.D. further away from the wild-type zone, coded by numbers above respective zones. Weighted positional scores are derived using this paradigm and presented in (B), with mean ± S.E.M. **, $p < 0.01$; one-way ANOVA followed by Bonferroni's multiple comparison test.

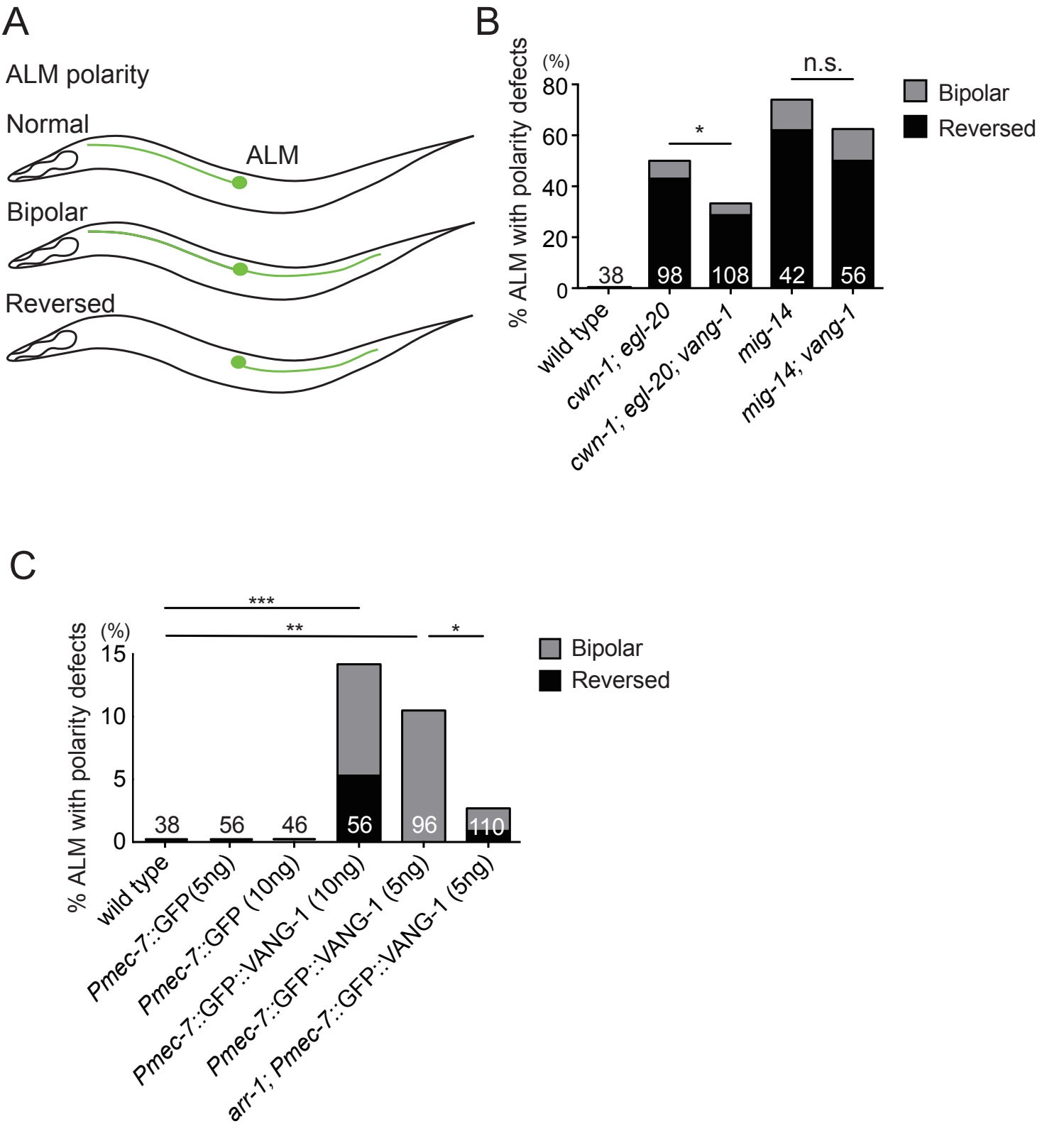

Fig. S3. *vang-1* antagonizes Wnt-Frizzled signaling in the polarization of the ALM neurons. (A) Schematic diagrams of wild-type and mutant ALM polarity. (B,C) Quantification of ALM polarity defects. N = neurons scored. *, $p < 0.05$, **, $p < 0.01$, ***, $p < 0.001$, n.s., not significant; two-proportion z test with Bonferroni corrections.

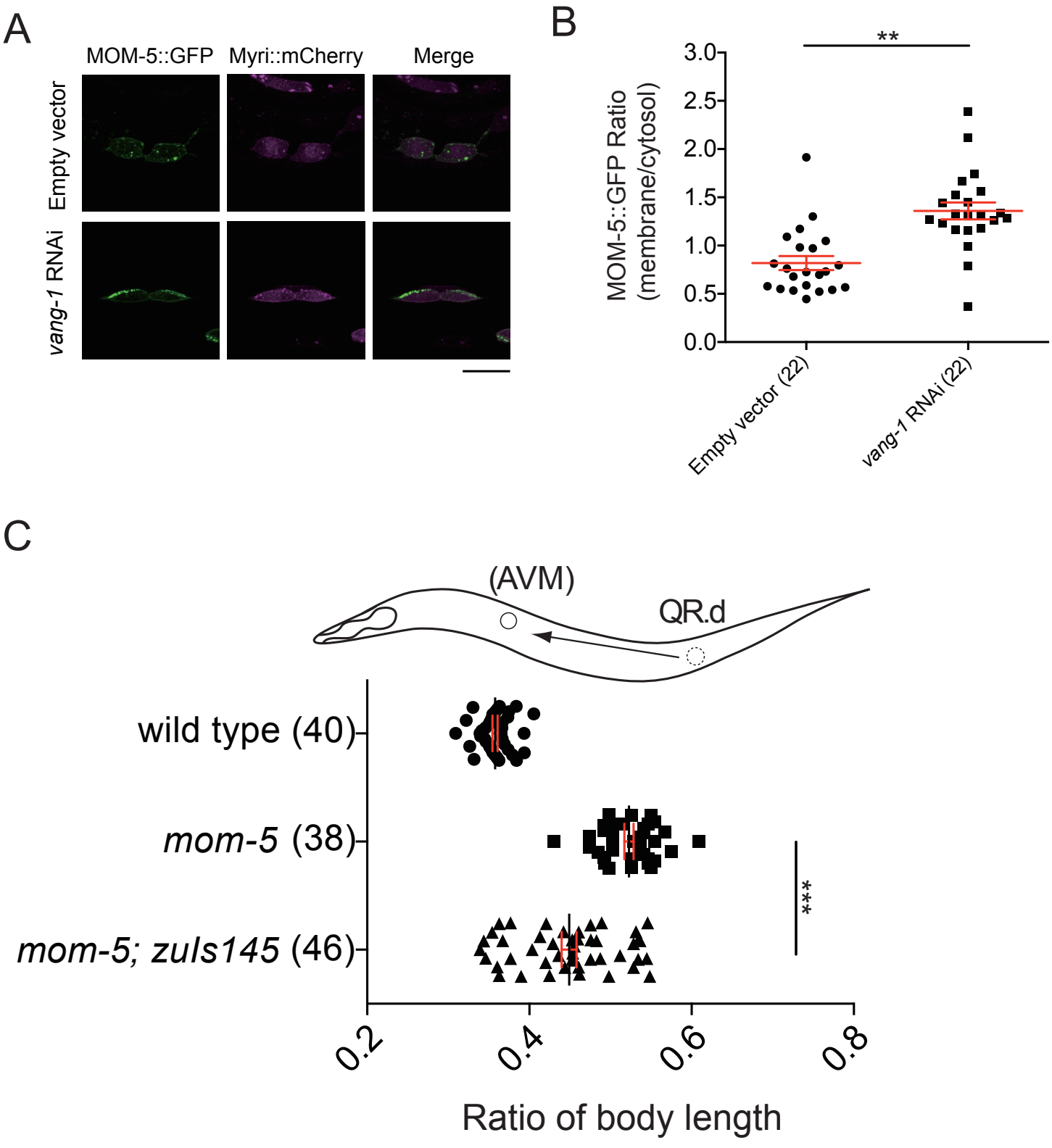

Fig. S4. *vang-1* regulates the distribution of functional MOM-5::GFP in QR.d. (A, B) Confocal projection images (A) and quantification of MOM-5::GFP distribution (B) in QR.d. MOM-5::GFP is from *zuIs145(Pnmy-2::MOM-5::GFP)* and the QR.d membrane marker is *rdvIs1(Pegl-17::Myri::mCherry)* with mCherry pseudocolored in magenta. Scale bar = 10 µm. Each dot represents a single neuron, with mean and S.E.M. indicated. N = neurons scored. **, $p < 0.01$; one-way ANOVA followed by Bonferroni's multiple comparison test. (C) Quantification of AVM positions along the anterior-posterior axis of the worm body. Each dot represents a single AVM neuron, with mean and S.E.M. indicated. N = neurons scored. ***, $p < 0.001$, one-way ANOVA followed by Bonferroni's multiple comparison test.

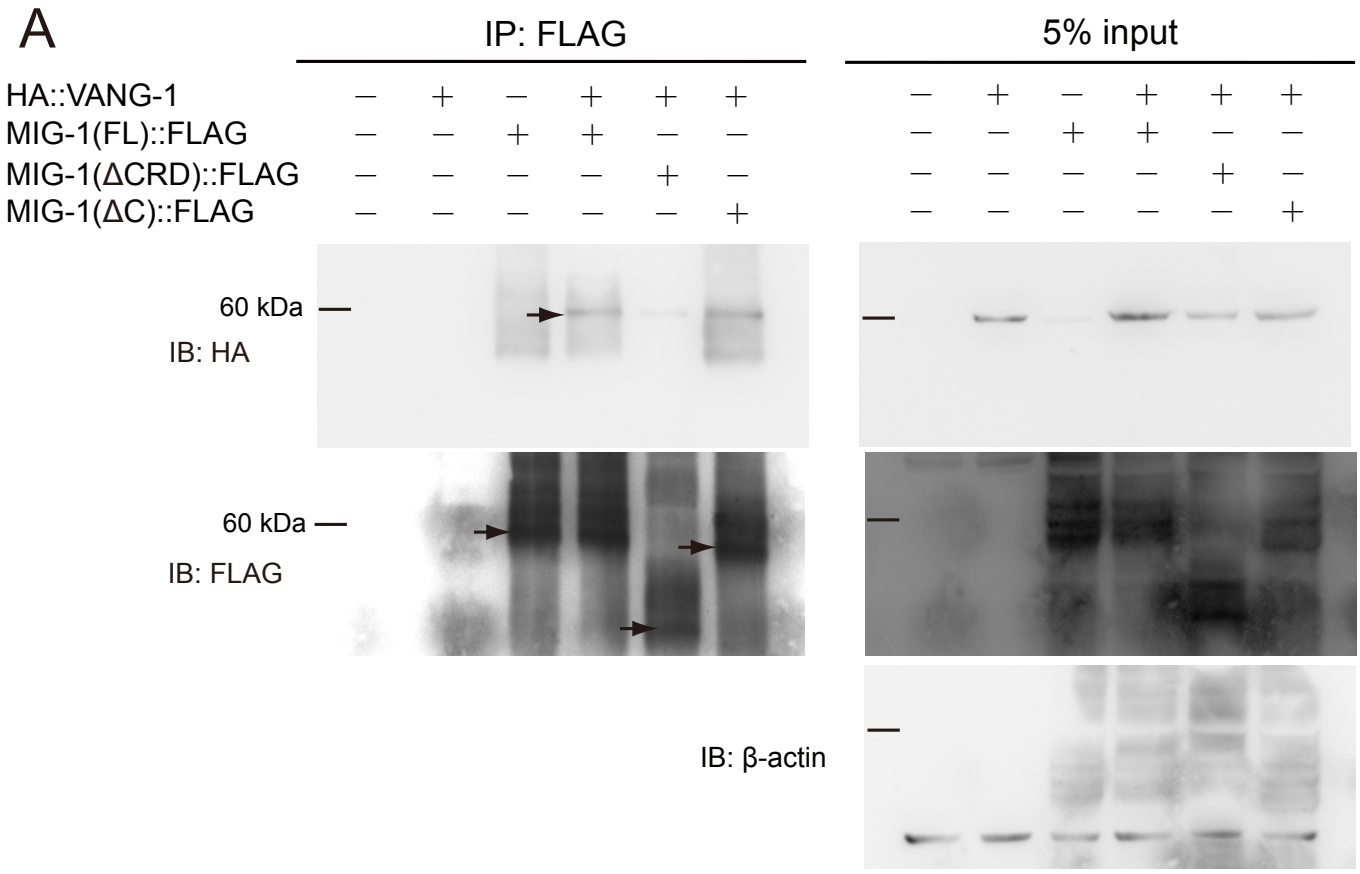

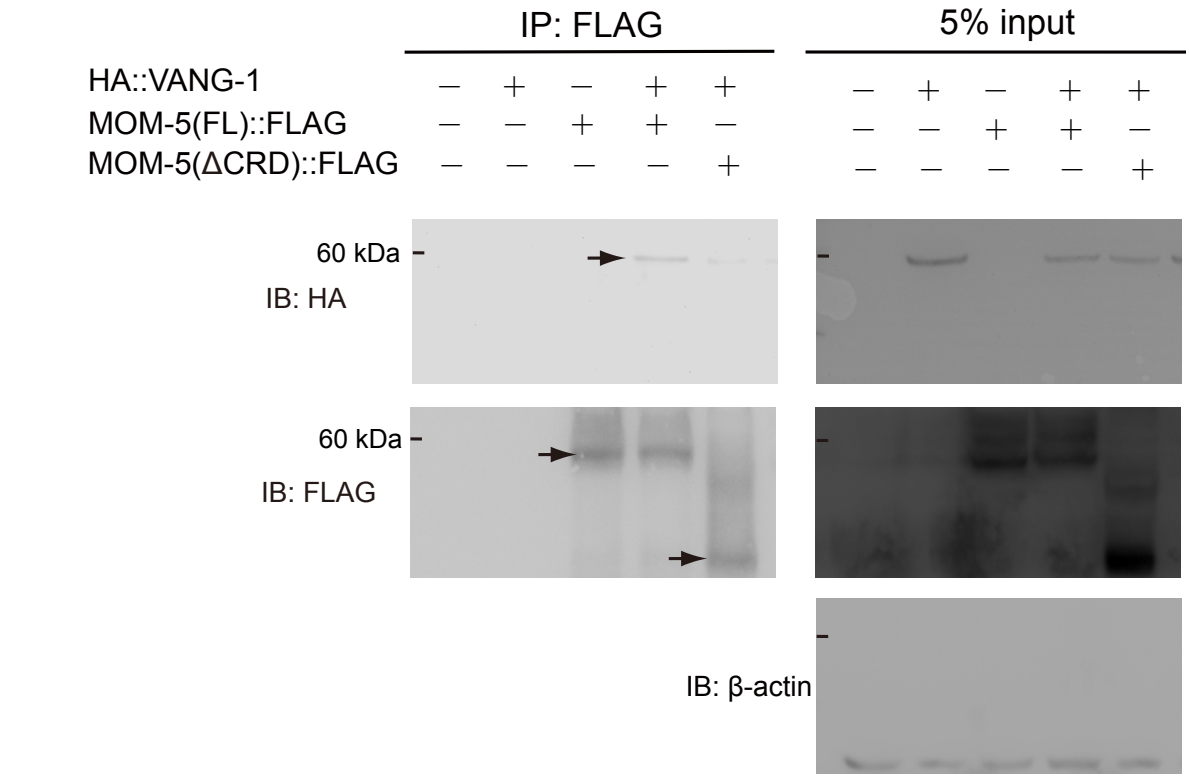

Fig. S5. Original western blotting membrane in co-immunoprecipitation experiments. The original, uncropped western blotting membranes for MIG-1 (A) and MOM-5 (B) co-immunoprecipitation experiments in Fig. 6B and 6C, respectively. FL, full-length. Arrows indicate MIG-1 and MOM-5 signals in respective immunoblots.

Table S1. *C. elegans* and bacterial strains, cell lines and antibodies used in the current study.

REAGENT or RESOURCE	SOURCE	IDENTIFIER
Bacterial Strains		
E. coli: Strain OP50	*Caenorhabditis Genetics Center (CGC)*	WormBase: OP50
Chemicals and Antibodies		
Antibody: anti-HA	Abcam	Abcam ab71113 (Duval et al., 2014)
Antibody: anti-FLAG	Sigma	Sigma F7425 (Lee et al., 2014)
Antibody: anti-β-actin	Santa Cruz	Santa Cruz sc- 47778 (Moloughney et al., 2018)
Experimental Models: Cell Lines		
HEK293	ATCC	ATCC: CRL-1573
Experimental Models: Organisms/Strains		
C. elegans: Strain N2: wild isolate	CGC	WormBase: N2
C. elegans: Strain CB3303: *mig-1(e1787) I*	CGC	WormBase: CB3303
C. elegans: Strain MT1306: *lin-17(n671) I*	CGC	WormBase: MT1306
C. elegans: Strain *mom-5(ne12) I*	lab of Craig Mello	N/A
C. elegans: Strain EW12: *mig-14(ga62) II*	CGC	WormBase: EW12
C. elegans: Strain RB763: *cwn-1(ok546) II*	CGC	WormBase: RB763
C. elegans: Strain SU352: *mig-5(rh147) II*	CGC	WormBase: SU352
C. elegans: Strain MT1215: *egl-20(n585) IV*	CGC	WormBase: MT1215

C. elegans: Strain *vang-1(tm1422)X*	Gian Garriga	N/A
C. elegans: Strain *vang-1(twn3)X*	This paper	N/A
C. elegans: Strain RB1125: *vang-1(ok1142) X*	CGC	WormBase:RB1125
C. elegans: Strain EW15: *bar-1(ga80) X*	CGC	WormBase:EW15
C. elegans: Strain RB660: *arr-1(ok401) X*	CGC	WormBase:RB660
C. elegans: Strain SK1006: *zdIs5[Pmec-4::GFP] I*	CGC	WormBase:SK1006
C. elegans: Strain CF453: *muIs16[mab-5::GFP + dpy-20(+)]II; dpy-20(e1282)IV*	CGC	WormBase:CF453
C. elegans: Strain RDV55: *rdvIs1v [Pegl-17::Myri-mCherry::pie-1 3'UTR + Pegl-17::mig-10::YFP::unc-54 3'UTR + Pegl-17::mCherry-TEV-S::his-24 + rol-6(su1006)]III*	CGC	WormBase:RDV55
C. elegans: Strain GR1366: *mgIs42[Ptph-1::GFP + pRF4(rol-6(su1006))]*	CGC	WormBase:GR1366
C. elegans: Strain JJ1992: *zuIs145[unc-119(+) +Pnmy-2::MOM-5::GFP]*	CGC	WormBase:JJ1992
C. elegans: Strain NG4978: *zdIs5; vang-1(tm1422)*	Gian Garriga	N/A
C. elegans: Strain NG6175: *zdIs5; arr-1(ok401)*	Gian Garriga/Jerome	N/A
C. elegans: Strain NG6407: *zdIs5 mig-1(e1787); arr-1(ok401)*	Gian Garriga/Jerome	N/A
C. elegans: Strain CLP293: *muIs16; rdvIs1*	This paper	N/A
C. elegans: Strain CLP392: *zdIs5; mig-5(rh147)*	This paper	N/A
C. elegans: Strain CLP463: *zdIs5; egl-20(n585); vang-1(tm1422)*	This paper	N/A

C. elegans: Strain CLP475: *zdIs5; bar-1(ga80) vang-1(tm1422)*	This paper	N/A
C. elegans: Strain CLP504: *zdIs5; cwn-1(ok546); rdvIs1; vang-1(tm1422)*	This paper	N/A
C. elegans: Strain CLP540: *muIs16; rdvIs1; vang-1(tm1422)*	This paper	N/A
C. elegans: Strain CLP570: *mig-1(e1787); muIs16; rdvIs1; vang-1(tm1422)*	This paper	N/A
C. elegans: Strain CLP571: *muIs16; rdvIs1; egl-20(n585)*	This paper	N/A
C. elegans: Strain CLP580: *muIs16; rdvIs1; egl-20(n585); vang-1(tm1422)*	This paper	N/A
C. elegans: Strain CLP598: *zdIs5 mom-5(ne12)/hT2*	This paper	N/A
C. elegans: Strain CLP605: *zdIs5 mom-5(ne12)/hT2; vang-1(tm1422)*	This paper	N/A
C. elegans: Strain CLP607: *zdIs5; bar-1(ga80)*	This paper	N/A
C. elegans: Strain CLP652: *zdIs5; twnEx230[Pmec-7::gfp::vang-1, Pdpy-30::NLS::DsRed]*	This paper	N/A
C. elegans: Strain CLP702: *zdIs5 mom-5(ne12)/hT2; zuIs145*	This paper	N/A
C. elegans: Strain CLP721: *vang-1(tm1422); mgIs42*	This paper	N/A
C. elegans: Strain CLP734: *zdIs5 mom-5(ne12)/hT2; rdvIs1*	This paper	N/A
C. elegans: Strain CLP737: *zdIs5 mom-5(ne12)/hT2; rdvIs1; vang-1(tm1422)*	This paper	N/A
C. elegans: Strain CLP853: *zdIs5 mig-1(e1787) mom-5(ne12); twnEx199[Punc-86::gfp, Pttx-3::gfp]*	This paper	N/A
C. elegans: Strain CLP863: *zdIs5; mig-5(rh147)/mInI; vang-1(tm1422)*	This paper	N/A

C. elegans: Strain CLP867: *zdIs5 mig-1(e1787); vang-1(ok1142)*	This paper	N/A
C. elegans: Strain CLP870: *zdIs5 mig-1(e1787); twnEx173[Pegl-17::gfp::vang-1, Pgcy-8::mcherry]*	This paper	N/A
C. elegans: Strain CLP871: *zdIs5; twnEx173[Pegl-17::gfp::vang-1, Pgcy-8::mcherry]*	This paper	N/A
C. elegans: Strain CLP872: *zdIs5; arr-1(ok401); twnEx173[Pegl-17::gfp::vang-1, Pgcy-8::mcherry]*	This paper	N/A
C. elegans: Strain CLP874: *zdIs5; mig-14(ga62); vang-1(tm1422); mgIs42*	This paper	N/A
C. elegans: Strain CLP875: zdIs5 mig-1(e1787) mom-5(ne12); vang-1(tm1422); twnEx199[Punc-86::gfp, Pttx-3::gfp]	This paper	N/A
C. elegans: Strain CLP876: *arr-1(ok401); mgIs42*	This paper	N/A
C. elegans: Strain CLP877: egl-20(n585)*; vang-1(tm1422); mgIs42; twnEX340[Punc-86::gfp::vang-1]*	This paper	N/A
C. elegans: Strain CLP878: zdIs5; *twnEx341[Pmec-7::gfp, Pdpy-30::NLS::dsRed](10ng)*	This paper	N/A
C. elegans: Strain CLP879: zdIs5; *twnEx342[Pmec-7::gfp, Pdpy-30::NLS::dsRed]*	This paper	N/A
C. elegans: Strain CLP930: *zdIs5; cwn-1(ok546)*	This paper	N/A
C. elegans: Strain CLP996: *egl-20(n585); mgIs42*	This paper	N/A
C. elegans: Strain CLP999: *mig-1(e1787); vang-1(tm1422); mgIs42*	This paper	N/A
C. elegans: Strain CLP1000: *mig-1(e1787); mgIs42*	This paper	N/A
C. elegans: Strain CLP1004: *egl-20(n585); arr-1(ok401) vang-1(tm1422); mgIs42*	This paper	N/A

C. elegans: Strain CLP1005: *egl-20(n585); arr-1(ok401); mgIs42*	This paper	N/A
C. elegans: Strain CLP1018: *cwn-1(ok546); egl-20(n585); vang-1(tm1422); mgIs42*	This paper	N/A
C. elegans: Strain CLP1021: zdIs5 mig-1(e1787); arr-1(ok401) vang-1(tm1422)	This paper	N/A
C. elegans: Strain CLP1025: *zdIs5; egl-20(n585); arr-1(ok401); mgIs42*	This paper	N/A
C. elegans: Strain CLP1041: *rdvIs1; zuIs145*	This paper	N/A
C. elegans: Strain CLP1043: *cwn-1(ok546); egl-20(n585); mgIs42*	This paper	N/A
C. elegans: Strain CLP1063: *zdIs5 mig-1(e1787) lin-17(n671)*	This paper	N/A
C. elegans: Strain CLP1064: *zdIs5 mom-5(ne12)/hT2; arr-1(ok401)*	This paper	N/A
C. elegans: Strain CLP1065: *mig-1(e1787); muIs16; rdvIs1*	This paper	N/A
C. elegans: Strain CLP1079: *zdIs5 mig-1(e1787) lin-17(n671); vang-1(tm1422)*	This paper	N/A
C. elegans: Strain CLP1081: *zdIs5 mig-1(e1787); twnEx464[Pegl-17::Cas9, Pu6::vang-1(sgRNA)]*	This paper	N/A
C. elegans: Strain CLP1082: *zdIs5 lin-17(n671)*	This paper	N/A
C. elegans: Strain CLP1089: *zdIs5 lin-17(n671); vang-1(tm1422)*	This paper	N/A
C. elegans: Strain CLP1096: *zdIs5 mig-1(e1787); rdvIs1; vang-1(twn3) zuIs145*	This paper	N/A

C. elegans: Strain CLP1100: *rdvIs1; zuIs145; twnEX482[Pegl-17::HA::VANG-1::SL2::BFP]*	This paper	N/A
C. elegans: Strain CLP1120: *rdvIs1; vang-1(twn3) zuIs145*	This paper	N/A
C. elegans: Strain CLP1163: *rdvIs1; arr-1(twn10) zuIs145*	This paper	N/A

Reference

Duval, N., Daubas, P., Bourcier De Carbon, C., St Cloment, C., Tinevez, J. Y., Lopes, M., Ribes, V. & Robert, B. (2014). Msx1 and Msx2 act as essential activators of Atoh1 expression in the murine spinal cord. *Development,* **141,** 1726-36.

Lee, J. H., Daugharthy, E. R., Scheiman, J., Kalhor, R., Yang, J. L., Ferrante, T. C., Terry, R., Jeanty, S. S., Li, C., Amamoto, R., Peters, D. T., Turczyk, B. M., Marblestone, A. H., Inverso, S. A., Bernard, A., Mali, P., Rios, X., Aach, J. & Church, G. M. (2014). Highly multiplexed subcellular RNA sequencing in situ. *Science,* **343,** 1360-3.

Moloughney, J. G., Vega-Cotto, N. M., Liu, S., Patel, C., Kim, P. K., Wu, C. C., Albaciete, D., Magaway, C., Chang, A., Rajput, S., Su, X., Werlen, G. & Jacinto, E. (2018). mTORC2 modulates the amplitude and duration of GFAT1 Ser243 phosphorylation to maintain flux through the hexosamine pathway during starvation. *J Biol Chem*, **293,** 16464-16478.

Table S2. Sequences of primers used in the cloning of *vang-1*, *mig-1* and *mom-5*.

Primer names	Sequences
pcDNA HA vang-1 KpnI F	GGTACCATGTACCCATACGATGTTCCAGATTAC
pcDNA HA vang-1 Age I R	ACCGGTTCAAACTGCCGACTCATTGC
kpnI mig-1CRDF	GCTAGCATGAATGAGCAAGGAGCAATTCAAGA
mig-1CRDMF	AATGAGCAAGGAGCAATTCAAGA
mig-1CRDMR	TCTTGAATTGCTCCTTGCTCATT
CRDmig-1MR2	CTGCCCGTCCACACCAATC
CRDmig-1MF2	ATTGGTGTGGACGGGCAGAATGAGCAAGGAGCAATTCAAGATG
mig-1DeleteCF	CTACGCGTCGACGTTTCGATAGTAAAATAT GATTTTACCGGTACCA G
mig-1DeleteCR	CTGGTACCGGTAAAATCATATTTTACTATCGAAACGTCGACGCGTA G
pcDNA mig-1 BamHI F	GGATCCATGGGACCATTTCGTGGTTACCTCG
mig-1C kpnI FLAG R	GGTACCTTACTTGTCGTCATCGTCTTTGTAGTCTCGAAACGTCGACG CGTAGGTG
pcDNA mig-1 FLAG KpnI F	GGTACCATGGGACCATTTCGTGGTTACC
pcDNA mig-1 FLAG AgeI R	ACCGGT TTACTTGTCGTCATCGTCTTTGTAGTCAATCATATTATTAG TTCGAAACGTC
SalI MOM-5 R	GTCGACCCTCATATTAACCTGATCAAC
smaI MOM-5 F	CCCGGGATGCATCGACATATTCTGATAT
SalIMOM-5 RR	GTCGACGGAGTATAATTGGACTAGTTGTACTC
MOM-5 CRD MR	AGTTGCTCGACTCGCTTCGAGTTGTTGAGAAT
MOM-5 MF	AGCGAGTCGAGCAACTCTAA

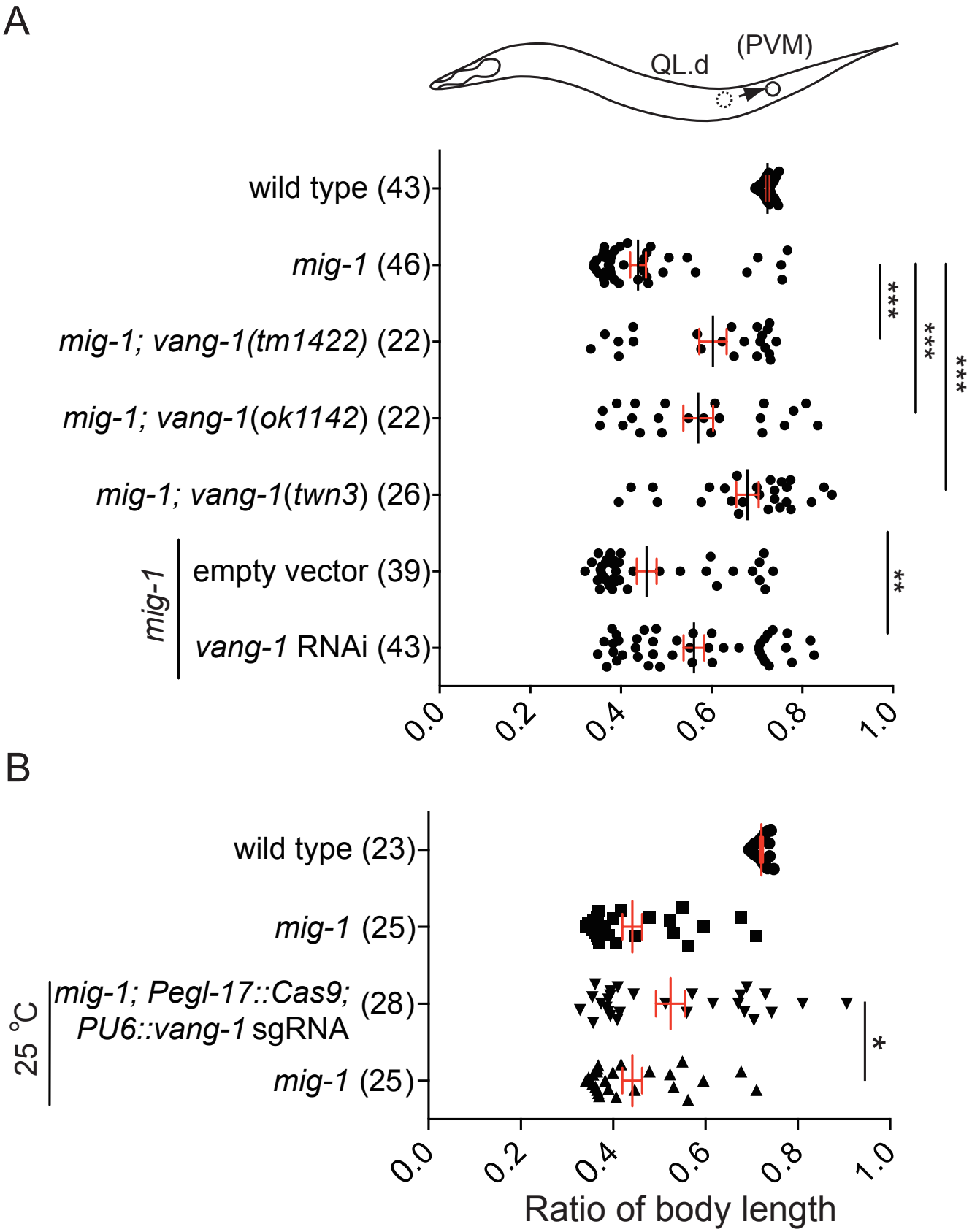

Fig. S1. *vang-1* antagonizes *mig-1* signaling in the migration of QL.d in *C. elegans*.

(A, B) Quantification of PVM positions along the anterior-posterior axis of the worm body. Each dot represents a single PVM neuron, with mean and standard errors of mean (S.E.M.) indicated. N = neurons scored. *, $p < 0.05$, **, $p < 0.01$, ***, $p < 0.001$; one-way ANOVA followed by Bonferroni's multiple comparison test.

A

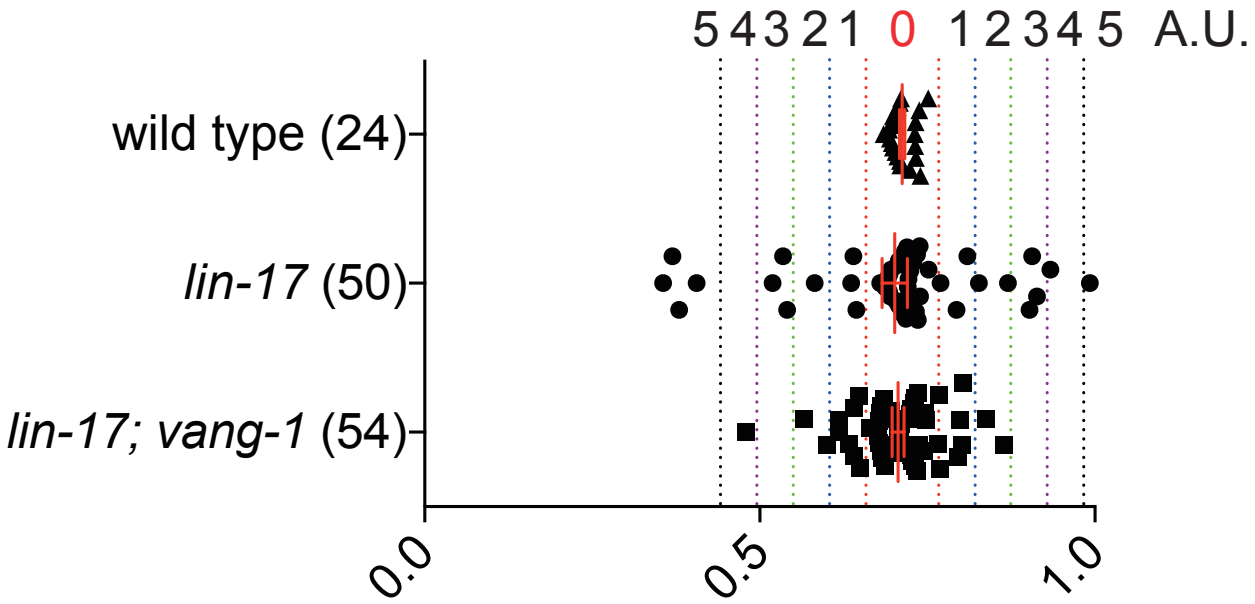

B

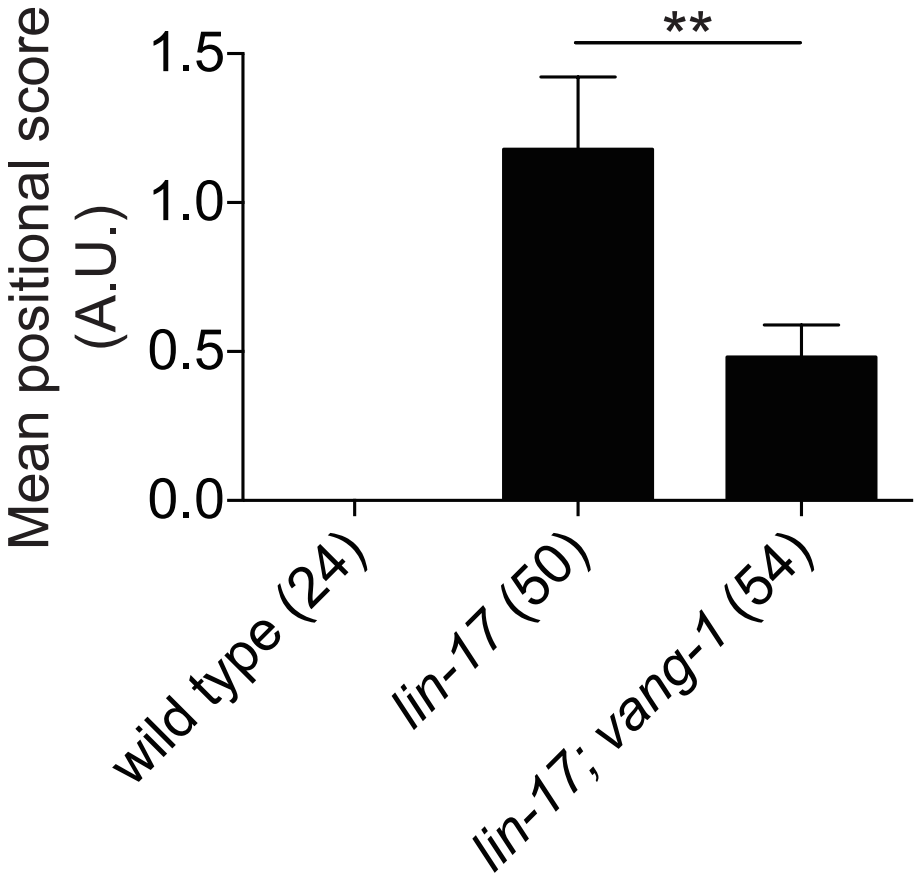

Fig. S2. *vang-1* antagonizes *lin-17* signaling in the migration of QL.d in *C. elegans*. (A) Quantification of PVM positions along the anterior-posterior axis of the worm body. Each dot represents a single PVM neuron, with mean and standard errors of mean (S.E.M.) indicated. N = neurons scored. PVM positions are quantified based on their deviation from the wild-type zone (defined by the red dotted lines, mean ± 3 S.D.) Each zone represents a distance of 3-S.D. further away from the wild-type zone, coded by numbers above respective zones. Weighted positional scores are derived using this paradigm and presented in (B), with mean ± S.E.M. **, $p < 0.01$; one-way ANOVA followed by Bonferroni's multiple comparison test.

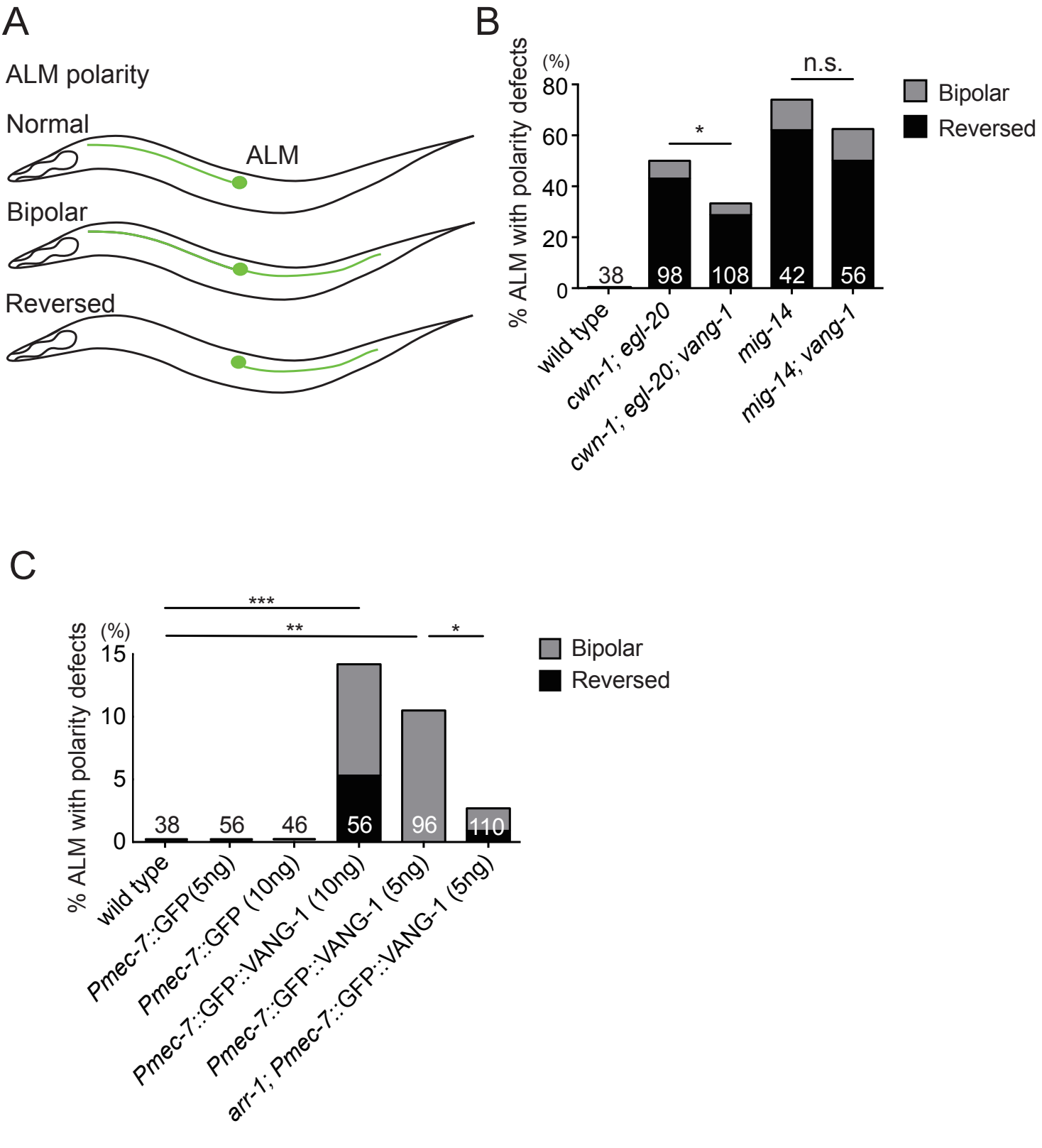

Fig. S3. *vang-1* antagonizes Wnt-Frizzled signaling in the polarization of the ALM neurons. (A) Schematic diagrams of wild-type and mutant ALM polarity. (B,C) Quantification of ALM polarity defects. N = neurons scored. *, $p < 0.05$, **, $p < 0.01$, ***, $p < 0.001$, n.s., not significant; two-proportion z test with Bonferroni corrections.

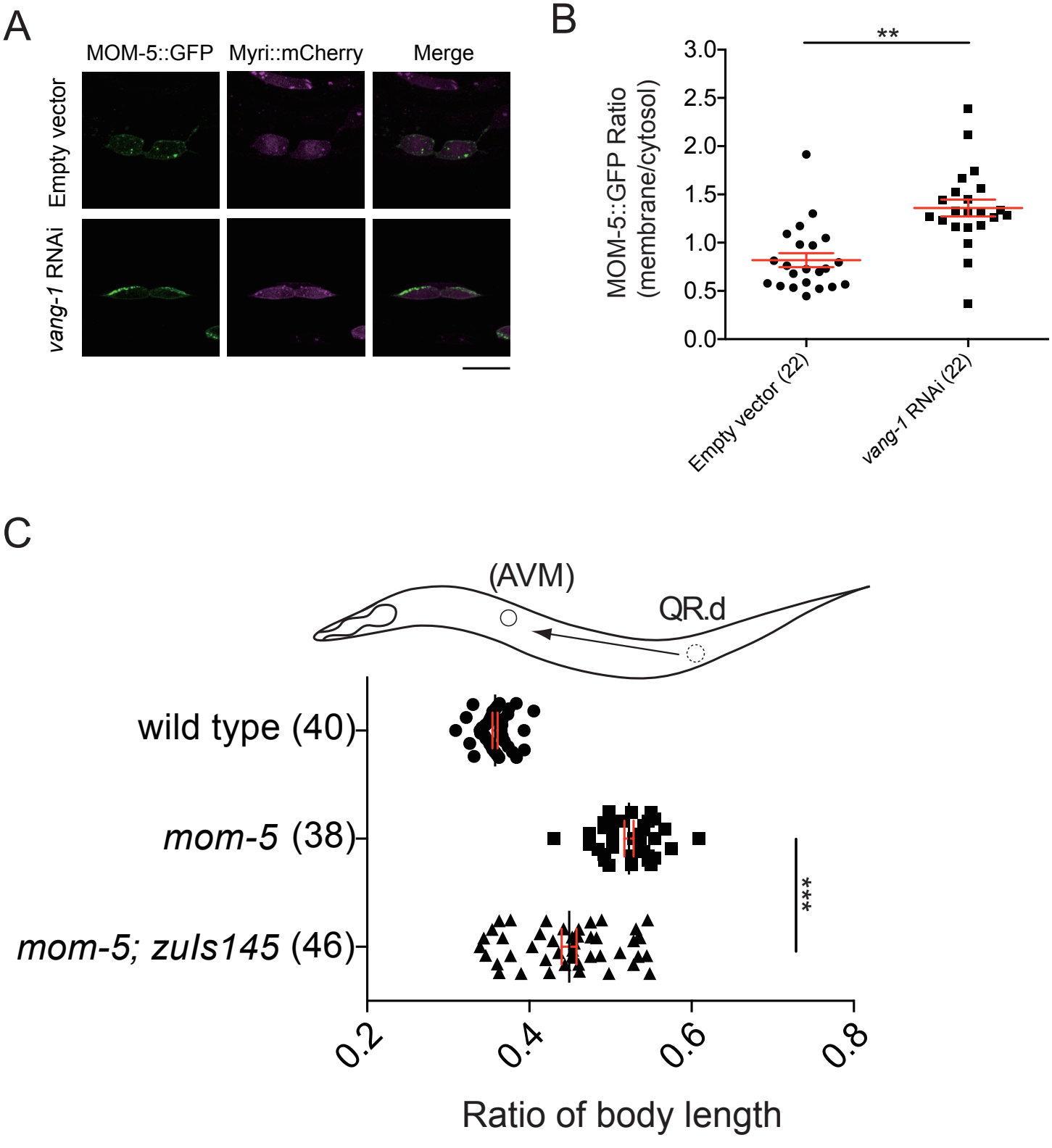

Fig. S4. *vang-1* regulates the distribution of functional MOM-5::GFP in QR.d. (A, B) Confocal projection images (A) and quantification of MOM-5::GFP distribution (B) in QR.d. MOM-5::GFP is from *zuIs145(Pnmy-2::MOM-5::GFP)* and the QR.d membrane marker is *rdvIs1(Pegl-17::Myri::mCherry)* with mCherry pseudocolored in magenta. Scale bar = 10 µm. Each dot represents a single neuron, with mean and S.E.M. indicated. N = neurons scored. **, $p < 0.01$; one-way ANOVA followed by Bonferroni's multiple comparison test. (C) Quantification of AVM positions along the anterior-posterior axis of the worm body. Each dot represents a single AVM neuron, with mean and S.E.M. indicated. N = neurons scored. ***, $p < 0.001$, one-way ANOVA followed by Bonferroni's multiple comparison test.

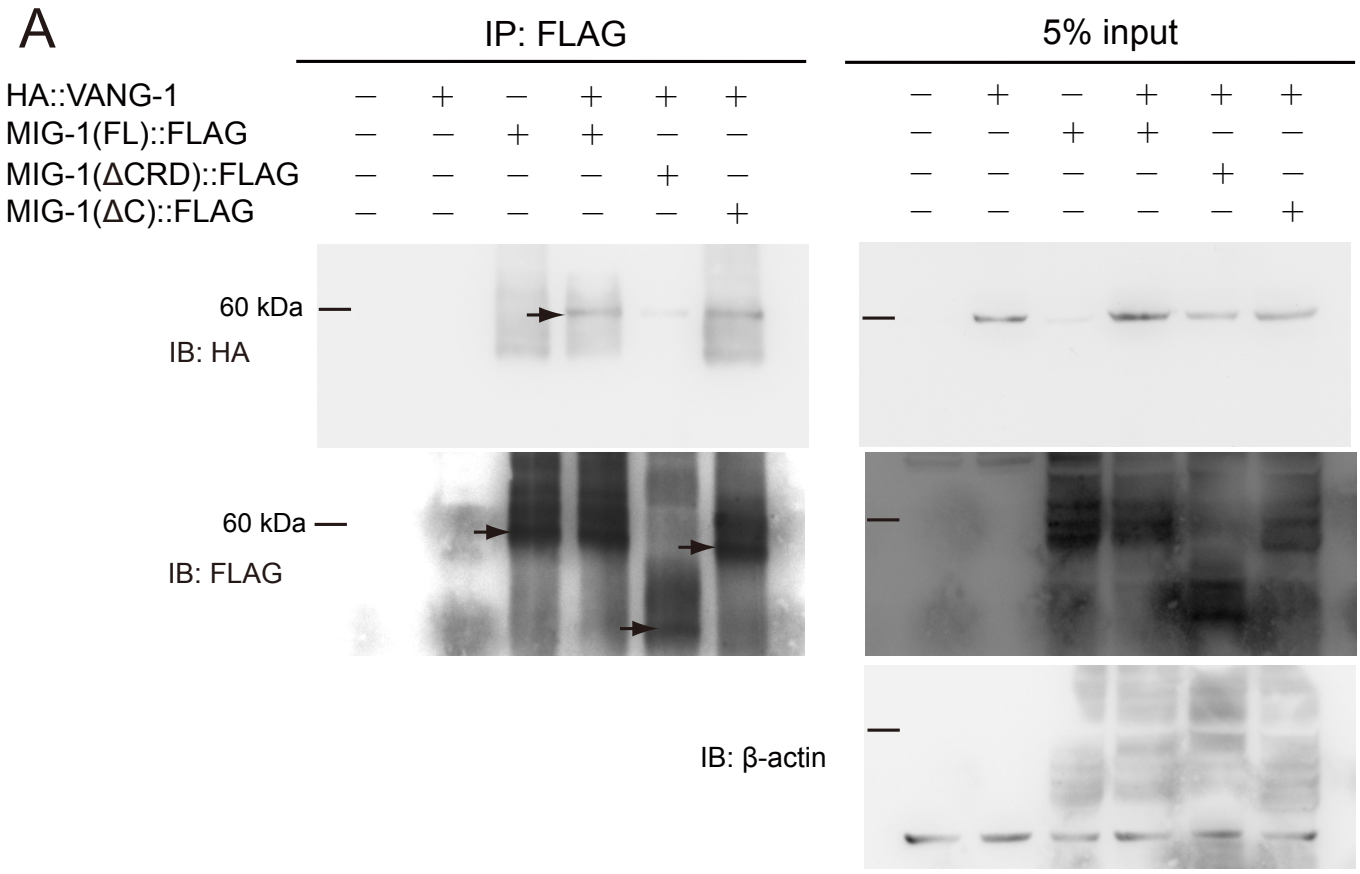

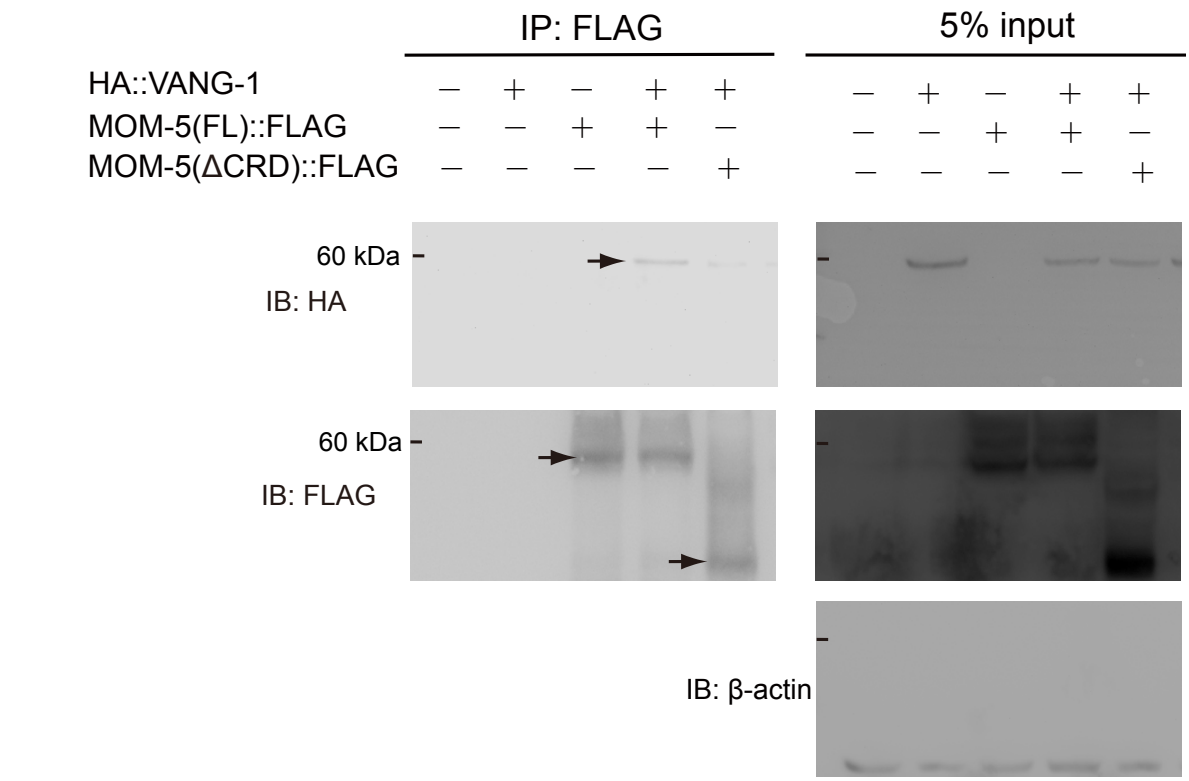

Fig. S5. Original western blotting membrane in co-immunoprecipitation experiments. The original, uncropped western blotting membranes for MIG-1 (A) and MOM-5 (B) co-immunoprecipitation experiments in Fig. 6B and 6C, respectively. FL, full-length. Arrows indicate MIG-1 and MOM-5 signals in respective immunoblots.